R. & M. No. 3661

R. & M. No. 3661

MINISTRY OF AVIATION SUPPLY

AERONAUTICAL RESEARCH COUNCIL
REPORTS AND MEMORANDA

Measurements of Section Pressure Distribution at a Mach Number of 2·0 on a Wing of 70 degrees Sweep Mounted on a Waisted Body

By K. G. WINTER and K. G. SMITH
Aerodynamics Dept., R.A.E., Bedford

LONDON: HER MAJESTY'S STATIONERY OFFICE
1971
PRICE £1·15 NET

Measurements of Section Pressure Distribution at a Mach Number of 2·0 on a Wing of 70 degrees Sweep Mounted on a Waisted Body

Reports and Memoranda No. 3661*
May, 1968

Summary.
The measurements were of pressure distribution at one section of the wing and along the wing-body junction of a half model. The wing was of STAC 11 section (12 per cent thick normal to the leading edge and of roof-top upper-surface design pressure distribution). The chord Reynolds numbers of the tests were from 1·4 to 5·7 million. Results at the lowest Reynolds number are of doubtful value because of uncertainty of the boundary layer condition. At higher Reynolds number the wing pressure correlate fairly well, on a basis of conditions normal to the leading edge, with those on the same model with wing set at 60 degrees sweep, and with two-dimensional section results but small differences lead to an increase in pressure drag. The wing-body junction pressure distribution is inadequately predicted by the design method used.

*Replaces R.A.E. Technical Report 68 114—A.R.C. 31 322.

LIST OF CONTENTS

1. *Introduction.*

The brief tests described in this Report are an extension of a series of tests on wings of 60 degrees sweep. A series of models was made to study the pressure distribution on wings designed to maintain sub-critical flow at a Mach number of 1·2. Half models which included a body were used, with the pressure-plotting station chosen to be well outboard to minimise the effect of wing root disturbances, so that the flow could be considered to be that over an infinite swept wing. The tests on the first of three models are described by Lawlor[1]. The first model had a thickness chord ratio of 18 per cent normal to the leading edge and 'triangular' pressure distribution at the design incidence. Subsequent models were designed for 'roof top' pressure distribution and were of 18 and 12 per cent thickness chord ratio. The latter of these was used in the present tests, with the wing root fixing modified to increase the angle of sweep to 70 degrees. The aims of the test, run at a Mach number of 2·0, were to study whether pressure distributions similar to those already measured at 60 degrees sweep would be maintained at the higher angle of sweep, with equivalent conditions normal to the leading edge, and to look at the effect of Reynolds number which it was considered might be more significant because of the increased boundary-layer outflow.

The tests were made in the 8ft × 8ft wind tunnel in April 1963.

2. *Description of Model and Test Procedure.*

Fig. 1 shows the arrangement of the model and Fig. 2 is a photograph of it in the tunnel. The model was mounted on a turntable in the starboard wall with the tip supported by cables to the roof and floor of the tunnel. The support was considered a necessary safety precaution in case of an emergency stop of the tunnel but also served to limit the deflection of the wing under steady conditions.

The wing is of constant section of form STAC 11[2], and is 12 per cent thick normal to the leading edge. The thickness distribution for this section is basically that of RAE 103[3], i.e. the maximum thickness is at 39 per cent chord, but a modification was made to the lower surface aft of 57·4 per cent chord by replacing, with a straight line, the concavity introduced by the camber. The camber has a maximum of 2·24 per cent chord at 47 per cent chord. Ordinates are given in Table 1. The tip is of parabolic planform designed to terminate streamwise at 60 degrees sweep, and the pressure-plotting station is far enough inboard to be uninfluenced by the tip shape. Because the wing was designed for 60 degrees sweep the pressure plotting station, as shown in Fig. 1, is inclined at 10 degrees to the freestream direction. The chordwise positions of the pressure-plotting holes, of 0·03 in diameter, are given with results in Tables 3 to 5. The unperturbed Mach line from the wing root trailing edge crosses the pressure-plotting station at roughly 20 per cent chord. A transition trip of 0·010 in ballotini, with about 400 particles per square inch, in a film of adhesive, was applied to both surfaces extending between 5 and 7 per cent chord.

The basic body is of 2·4 in radius and was mounted on a block of rectangular section. The thickness of the block was made proportional to the body radius, to avoid a strong disturbance at the nose. It tapers in thickness from zero at the nose to 2 in where the body is parallel, and its thickness there approximates to the tunnel wall boundary-layer displacement thickness. The body is shaped differentially between the upper and lower surfaces at the wing root. The aim was to produce in the root the same pressure distribution as would exist over an infinite sheared wing at $C_L = 0{\cdot}04$ at $M = 2$, but physical limitations on the amount of waisting possible, and on fairing upper and lower surfaces together aft of the wing, resulted in a compromise in which, according to the calculations, the required roof-top pressure distribution would be maintained only up to about 30 per cent chord. The method used was that described by Bagley[4] in which upper and lower surfaces are treated as being separately half of symmetrical arrangements. The cross-sections were taken as quarter-ellipses with the body depth unchanged. The dimensions are listed in Table 2. Pressure-plotting holes were provided in the body round the wing root about 0·05 in away from the wing surface. The chordwise positions are given in the tables of results (Tables 6 to 8).

The tests were all made at a nominal Mach number of 2 at Reynolds numbers based on wing chord of 5·73, 2·86 and 1·44 million. The actual Mach numbers at the location of the wing pressure-plotting station, obtained from a calibration of the tunnel using pitot tubes, were 2·004, 2·000 and 1·996 at these Reynolds numbers respectively. Pressure at one station on the wing and in the wing body junction were measured on capsule manometers at values of incidence of $-0{\cdot}86$, 0, 1·3, 2·0 and 3·0 degrees. Pressure coefficients

were calculated from the measured pressures using the tunnel stagnation pressure and Mach number to define the free-stream static pressure and kinetic pressure. At an incidence of 2 degrees photographs of tufts attached to the wing were taken.

3. *Accuracy*

Inspection of the wing section at the pressure-plotting station showed that the wing was too full on the upper surface by a maximum of 0·005 in, and under-size on the lower surface by a maximum of 0·001 in (the maximum thickness is about 0·7 in). The error varied smoothly along the chord and was small at leading and trailing edges. At other stations errors up to twice those at the pressure-plotting station were present.

Estimates of possible pressure-coefficient errors have been made. The sources of error considered are measured local static pressure, datum static pressure, humidity (the frost-point of the air was always below $-27°C$) and pressure hole size. The total possible estimated errors in pressure coefficient are 0·008 at a Reynolds number of 1·44 million and 0·005 at 2·86 and 5·73 million. Examination of the results suggests that there may also be a systematic error varying with Reynolds number. As Reynolds number decreases there is an increase in the value of pressure coefficient. For example in Fig. 3f the pressure coefficient at $\frac{1}{2}$ per cent chord on the lower surface, which is roughly the stagnation point, increases from 0·131 at $Re_c = 5{\cdot}73$ million to 0·137 at 2·86 million and 0·145 at 1·44 million. For an infinite swept wing the maximum value of C_p would be 0·131. A value of 0·145 implies a reduction in the effective angle of sweep of 1 degree, or a decrease in the effective freestream Mach number of 0·02. Either of these explanations is unlikely (though there may be some scale effect on the interference between the body nose and the tunnel sidewall boundary layer resulting in downstream effects on the wing) and it has been assumed that there is an unexplained error in the static pressure measurements or in the datum static pressure determination. For consistency the values of C_p should be reduced by 0·006 at $Re_c = 2{\cdot}86$ million and by 0·014 at $Re_c = 1{\cdot}44$ million.

An approximate calculation of the deflection of the wing at the pressure plotting station due to aerodynamic loading gives an increase in incidence of 0·05 degrees at a nominal incidence of 3 degrees for the largest Reynolds number as a result of both torsion and bending. The values of incidence quoted are nominal and have a setting accuracy of about 0·02 degrees.

4. *Results and Discussion.*

The results are tabulated for the wing pressure-plotting station in Tables 3, 4, 5 and for the wing-body junction in Tables 6, 7, 8. They are presented in three forms, C_p the pressure coefficient, p/H_n the ratio of local static pressure to the total pressure of the flow normal to the leading edge, and as local Mach number derived from the measured pressure assuming isentropic flow.

Pressure coefficients for the wing station are plotted in Fig. 3 and for the wing-body junction in Fig. 14.

4.1. *Wing Pressure Distribution.*

The pressure distribution on the wing is shown in Figs. 3a to 3c. The essential point to be established in considering the change of pressure distribution with Reynolds number is the state of the boundary layer on the wing. Unfortunately time was not available during the tests for flow visualisation studies and no definite statement can be made. Also a common transition trip was used for all three Reynolds numbers. Applying the criterion established by Evans[5] for slender wings (subsequent to the completion of the experiment) transition would be expected to be at the roughness band only for the highest test Reynolds number. The effect of Reynolds number shown by the experiment therefore probably includes also the effect of varying transition position. Some evidence that this is so is shown in Figs. 3a and 3b, where the pressure distribution at 2 degrees incidence with and without tufts on the upper surface is compared. Photographs of the upper surface of the wing with tufts are given in Fig. 4. The tufts were of stranded nylon about 0·03 in diameter and were glued to the wing at 10 per cent chord and 10 per cent span intervals. They should therefore provide locally a more adequate transition trip than the ballotini. Whilst the photographs were being taken pressures were recorded at the highest and lowest Reynolds numbers. It

should be noted that time was not allowed for the manometers to stabilise, and at the lowest Reynolds number the absolute level of pressure indicated is certainly erroneous. Nevertheless it is clear from the change in shape of the pressure distribution that the tufts produce a major change in the flow over the wing at the lowest Reynolds number (1·44 million). There is little effect at the highest Reynolds number (5·73 million).

Schlieren photographs are shown in Fig. 5 for an incidence of 2 degrees with and without tufts on the wing. A large part of the wing is masked by the body but the last 25 per cent of the pressure-plotting station is visible between the base of the body and the wing tip support cables. The schlieren beam is of course transmitted through a spanwise extent of the flow over the wing (about $6\frac{1}{2}$ in) and through the wing and body wake so that the resulting picture is an integrated effect. Nevertheless the photographs do show differences in flow for different conditions compatible with the changes in pressure distribution. Without tufts the trailing-edge separation diminishes as the Reynolds number is reduced, and at the lowest Reynolds number it is not discernible and is replaced by what may be interpreted as a long bubble separation on the wing surface. With tufts the flow is not changed appreciably at the two higher Reynolds numbers but at the lowest Reynolds number the bubble separation is very much reduced if not totally eliminated.

The distribution at 1·44 million with tufts forms a logical sequence with 5·73 and 2·86 million without tufts rather than the complete change of character shown at 1·44 million without tufts. This sequence exhibits an adverse effect of Reynolds number in the sense that the trailing-edge separation on the upper surface increases with increase of Reynolds number. This is consistent with the tuft photographs in which there is an apparent diminution of the outflow near the trailing edge with decreasing Reynolds number, though there must be some reservation because of the changing effect of the stiffness of the tufts with decreasing pressure. (There is also some suggestion of an increased inflow over the forward part of the wing as Reynolds number decreases.)

Considering other values of incidence, at $-0{\cdot}86$ degrees (Fig. 3c) tests were made only at 5·73 and 2·86 million. On the upper surface, the effect of change of Reynolds number is small, but on the lower surface, where there is probably a shock between 5 and 10 per cent chord, increase of Reynolds number gives a steeper compression. This could be consistent with the flow being laminar at 2·86 million. At $\alpha = 0$ (Fig. 3d) apart from the general apparent increase of pressure with reduction of Reynolds number, noted in Section 3, there is a sharpening of the suction peak at mid-chord with increase of Reynolds number. The effects at 1·3 degrees incidence (Fig. 3e) are similar to those at 2 degrees. At 3 degrees incidence the equivalent two-dimensional pressure distribution (*see* Fig. 7) shows evidence of a shock on the upper surface at about 40 per cent chord. For the wing swept at 70 degrees at the highest Reynolds number the pressure rise through the shock is diffused into a steady recompression with considerable trailing edge separation. At 2·86 million the compression is steeper and occurs at about 50 per cent chord with little separation apparent at the trailing edge. This suggests that there is some separation occurring from say 30 per cent chord with reattachment before the trailing edge which implies a vortex type of flow. The behaviour is similar at the lowest Reynolds number but with reattachment occurring even further aft. The separation may be laminar with reduction in Reynolds number delaying transition in the separated layer and consequently delaying reattachment.

One aim of the experiment was to see whether, at the large angle of sweep of 70 degrees, flow conditions normal to the leading edge might still be equivalent to those over a two-dimensional section. It is necessary before making the comparison to consider whether the loading is unduly distorted by the wing root trailing edge disturbance which crosses the pressure plotting station at about 20 per cent chord. In Fig. 6 the incidence loading along the chord, as calculated by the conical flow methods of Cohen[6], is shown. The loading is plotted as the rate of change of pressure coefficient with incidence for a flat plate wing with no allowance made for the presence of the body. (On the basis of cross-flow past a cylinder the local lift-curve slope would be increased by about 2 per cent—*see* Table 9.) Outboard of the intersection of the root trailing edge Mach line and the leading edge of a swept wing the flow is near two-dimensional in character, though not in the magnitude of the leading edge singularity. Cohen provides charts for determining the strength of the singularity. Using her charts, and taking the value of the singularity at the intersection of the root trailing-edge Mach line and leading edge for the wing tested, i.e. at a station outboard of the pressure plotting station, the broken line in Fig. 6 is obtained. This can be seen to be quite close to the conical flow

distribution, (in fact the lift curve slope is 2 per cent larger). The influence of the wing apex on the character of the flow may thus be taken as being sufficiently small to make comparison with two-dimensional type flows justified.

The experimental loadings for both surfaces at $Re_c = 5{\cdot}73$ million taken between 0 and 2 degrees incidence have the same general shape as the calculated loading but show local effects. The leading-edge loading is not achieved but is compensated by an increased loading up to about 25 per cent chord. Root trailing edge disturbances crossing the pressure-plotting station both for 0 and 2 degrees incidence may be expected to appear in the curves of Fig. 6. The Mach number over the rear part of the wing is higher than freestream except for the lower surface at 2 degrees incidence when it is close to the freestream value. The disturbances will thus be, with this exception, aft of the linear theory position of about 20 per cent chord, and will be responsible for the irregular nature of the curves between 20 and 40 per cent chord. Trailing-edge separation causes the increased loading there on the upper surface and the decreased loading on the lower surface.

Comparison with measured pressure distributions for the wing swept at 60° and for a two-dimensional wing is shown in Fig. 7. The pressure is expressed as p/H_n where H_n is the total pressure of the flow normal to the leading edge. The comparison is made at two values of lift coefficient corresponding to approximately 0·6 and 0·85 for an unswept wing at a value of the Mach number normal to the leading edge of 0·68. Measurements at N.P.L. (unpublished) on a two-dimensional wing at a Mach number of 0·68 are sufficiently detailed to be interpolated to the actual values of $C_L \sec^2 \varphi$ of 0·609 and 0·854 obtained on the 70 degrees swept wing, and the interpolated values are plotted in Fig. 7. Also plotted are measurements at ARA on the wing at 60 degrees sweep at roughly comparable conditions. Transition was adequately fixed for both the zero and 60 degrees swept wings. Because of the uncertainty of transition fixing the results for the 70 degrees wing at the highest Reynolds number are used.

At $C_L \sec^2 \varphi \simeq 0{\cdot}6$ (Fig. 7a) the distributions at 0 and 60 degrees sweep show fairly good correspondence over the forward half of the wing but there is evidence of rear separation from about 75 per cent for the 60 degree swept wing. At 70 degrees sweep the separation spreads forward to about 70 per cent chord and the pressure recovery at the trailing edge deteriorates further. This separation produces extra lift, which, together with an increased loading forward on the lower surface, is compensated by a reduced level of the roof top pressure. At $C_L \sec^2 \varphi \simeq 0{\cdot}85$ (Fig. 7b) there are some differences. For the two-dimensional wing the super-critical suction level of the roof top is terminated by a shock at between 35 and 40 per cent chord. The pressure rise through the shock is accentuated at 60 degrees sweep but at 70 degrees is diffused into an almost uniform compression extending from 10 to 60 per cent chord. There is little or no evidence of a rear separation for the unswept wing but the separation at both 60 degrees and 70 degrees sweep now spreads forward to about 60 per cent chord with about the same level of trailing edge pressure recovery. The increased pressure over the forward part of the lower surface of the 70 degree wing occurs as at the lower lift coefficient.

In general the description of the flow over the swept wing in terms of conditions normal to the leading edge appears to be a valid concept. However, the criterion for rear separation clearly cannot be the same for the swept wings as for the two-dimensional wings. On the basis of the 'line of flow' principle[7] the pressure gradients controlling the boundary-layer development for comparable conditions as in Fig. 7 are reduced by the factor $\cos^2 \varphi$ for a wing swept at an angle φ compared with an unswept wing. Thus, in simple terms, a reduction of a tendency to separation with increasing sweepback might have been anticipated in contrast to the pronounced increase of the experimental results. This simple argument ignores the effect of the vorticity induced in the wake by the angle change at the trailing edge which may be an important feature of the flow on swept wings. It is unfortunate in the present experiments that the boundary-layer transition at the lower two Reynolds numbers cannot be regarded as fixed since the Reynolds number range covered is the same as that in the comparisons in Fig. 7. It would have been interesting to determine the effects of sweep and of Reynolds number.

4.2. *Section Lift and Drag.*

The measured pressures have been integrated to give lift and pressure drag as plotted in Figs. 8 and 9. As would be expected from the pressure distributions the lift curve slope decreases as Reynolds number

increases. The uncertainty of the boundary-layer condition makes it difficult to predict what the further effect of Reynolds number increase might be. The pressure drag shows little effect of Reynolds number at low lift but has a minimum for a given lift within the Reynolds number range covered as the lift increases. The latter effect is the result of the opposing changes produced by increase of Reynolds number in reducing the extended length of high suction level on the upper surface and in promoting rear separation, i.e. the effects of forward separation as opposed to rear separation. At a given incidence the drag decreases monotonically with increase of Reynolds number.

The lift, centre of pressure, and drag at the highest Reynolds number are compared in Figs. 10, 11, 12 with results at zero and 60 degrees sweep. The comparison is based on conditions normal to the leading edge for which the parameters are $\alpha \sec \varphi$, $C_L \sec^2 \varphi$ and $C_D \sec^3 \varphi$. Because both for 60 and 70 degrees sweep the pressure plotting station is not sufficiently far outboard for the loading to be considered (in magnitude) as that over an infinite sheared wing a direct comparison as in Fig. 10 is misleading. The following table compares measured and estimated lift-curve slopes.

TABLE 9

Comparison of Measured and Estimated Lift-Curve Slopes per Degree.

φ	0	60	70
$Re_c \times 10^6$	1·7	4·8	5·7
M_n	0·68	0·677	0·684
Flat plate $C_{L_\alpha} \sec \varphi$	0·1496	0·1134	0·1023
Thickness factor	1·069	1·069	1·069
Scale factor	0·784	0·824	0·830
Body upwash factor	1·0	1·011	1·023
Estimated $C_{L_\alpha} \sec \varphi$	0·1253	0·1009	0·0928
Measured $C_{L_\alpha} \sec \varphi$	0·1170	0·1078	0·0928
Measured $C_{L_\alpha} \sec \varphi$ corrected for wing deflection	0·1170	0·1041	0·0913
Ratio of measurement: estimate	0·934	1·032	0·985

In this table the flat plate estimate is taken as $\frac{2\pi}{57{\cdot}3}(1-M_n^2)^{-\frac{1}{2}}$ for $\varphi = 0$, as given by the approximate curves of Ref. 6 for $\varphi = 60$ degrees, and from integration of the conical flow loading shown in Fig. 6 for $\varphi = 70$ degrees. The thickness factor for $M = 0$ is taken from the section design calculations of Ref. 2, and is modified for compressibility by using the R.Ae.S. data sheets[8] (Wings 01.01.01). The scale factor is also taken from Ref. 8 by using the empirical curves of Wings 01.01.05 and assuming leading-edge transition. The section normal to the leading edge is taken but the stream-wise chord Reynolds number has been used. The body upwash factor is that for an infinite circular cylinder.

The final result is rather surprising in that the estimates are closer to the measurement for the swept sections than for the unswept section. The thickness corrections used are derived from experiments on unswept sections and will not strictly be applicable to swept wings. It may be that errors in these corrections compensate for possible errors in the flat plate estimates to give unjustifiably good final estimates. There is also room for different interpretations of the lift-incidence curves. The slopes quoted above are those of the lines drawn on Fig. 10. These are 'least squares' lines for incidence less than 6 degrees. The

slope of a line through the lowest two points for the unswept wing has, in fact, a value about 7 per cent above the estimate.

The other feature of Fig. 10 which calls for comment is the large change of incidence for zero lift with increase of angle of sweep. The 'least squares' lines for the data show increases in incidence for zero lift compared with that obtained by extrapolation of the section design calculations[2] of 0·1, 0·3 and 1·4 degrees for angles of sweep of 0, 60 and 70 degrees respectively. The wing at 60 degrees sweep was also tested with vortex generators on the upper surface. In this condition the incidence for zero lift decreased by 0·4 degrees and the lift-curve slope increased by 14 per cent so that the measurements are in close agreement with an inviscid calculation. The implication is that the change in incidence for zero lift is a viscous effect. It might be noted that for the section of Ref. 1 tested at 60 degrees sweep the incidence for zero lift was 0·8 degree greater than predicted by calculation for inviscid incompressible flow.

Fig. 11 shows close agreement of centre of pressure position for the unswept and 70 degree swept wings at corresponding lift coefficients despite the changes in pressure distribution seen in Fig. 7.

Pressure drag coefficients are plotted against lift in Fig. 12. For 60 degrees sweep the drag is only slightly greater than for the unswept wing in the region of overlap of the results and when the trailing edge separation is small. At the largest lift coefficient the separation (Fig. 7b) leads to appreciably higher drag. For 70 degrees sweep the drag at zero lift is about twice that for 60 degrees sweep and increases rapidly with increase of lift. Part of this increase arises from the lower lift-curve slope for 70 degrees sweep and from the changed incidence for zero lift. A clearer comparison is given in Fig. 13 where the chordwise force coefficient is plotted against normal force coefficient. The shape of the curve for 60 degrees sweep has been inferred from Figs. 10 and 12. The results for 70 degrees sweep are now more nearly parallel with the curves for zero and 60 degrees sweep. At the highest normal force coefficient where there is extensive trailing edge separation for both 60 and 70 degrees sweep the values of chord force coefficient are fairly close. A comparison of this sort is, of course, very sensitive to any buoyancy effects on the chord force evaluation. For the conditions of the tests at 70 degrees sweep calibration of the empty tunnel showed an adverse velocity gradient amounting to about $\frac{1}{4}$ per cent change in Mach number over the pressure-plotting station. The estimated correction to $C_c \sec^2 \varphi$ for this change is an increase of about 0·002. The large increase in $C_c \sec^2 \varphi$ for 70 degrees sweep is therefore unlikely to be due to buoyancy effect though the flow field of the body has not been considered. It appears to arise primarily from reduction of the suction on the upper surface forward of the crest with an increasing effect of trailing edge separation as incidence increases.

4.3. *Wing-Body Junction Pressure Distribution.*

The pressure distribution along the wing-body junction is shown in Fig. 14. The distribution is compared with calculations for upper and lower surfaces in Figs. 14b and 14c at $\alpha = 0$. The calculations used the method proposed by Bagley[4] in which the body side is treated as a reflection plane in obtaining the wing-velocity field and the velocity field of the body is added separately. The experiments show that the predicted pressure distribution is not achieved except towards the trailing edge. For the most part, the experimental points lie between the predictions for the wing alone and for the total. A rough approximation to the measurements could be obtained by adding about half the calculated body field to the wing field. However, the reflection plate assumption for the wing field calculations is probably more questionable than the additive effect of the body waisting and progress in wing-body junction design methods is more likely to come from improvement in the understanding of the basic flow for a wing with a cylindrical body rather than from such crude empirical factors. Further evidence of the inadequacy of the assumption is shown in the incidence loading (Fig. 15). The loading over the forward part of the root section is almost double the uniform loading predicted by conical flow theory[6].

5. *Conclusions.*

(1) Pressure distributions on the wing show marked scale effects. Though no direct determination of transition position was made it is inferred from the results that at the lowest Reynolds number (1·4 million) the boundary-layer transition trip was inadequate.

(2) Pressure distributions in terms of the flow normal to the leading edge correlate fairly well with results for an unswept wing and for the same wing at 60 degrees sweep. Trailing edge separation increases with increases of sweep. At high angles of incidence the sharp pressure rise, obtained for 0 and 60 degrees sweep, associated with the shock wave terminating a supersonic region becomes a diffuse recompression at 70 degrees sweep.

(3) The lift curve slope can be predicted fairly well from a combination of linear theory and two-dimensional section data. The angle of incidence for zero lift is however increased, as also found in Ref. 1.

(4) The section pressure drag is considerably greater for 70 degrees sweep than for 0 or 60 degrees.

(5) The wing-body junction pressure distribution is inadequately predicted by the design method used.

Acknowledgements.

The authors are grateful to Mr. T. E. Bateman of the Aircraft Research Association for unpublished results of the model tested at 60 degrees sweep and to Mr. H. H. Pearcey of the National Physical Laboratory for the results of section tests on the STAC 11 section.

LIST OF SYMBOLS

c	Wing chord (streamwise)
C_L	Lift coefficient
C_{L_α}	Lift-curve slope per degree
C_D	Drag coefficient
C_c	Chordwise-force coefficient
C_N	Normal-force coefficient
C_p	Pressure coefficient
H_n	Total pressure of flow normal to wing leading edge
M	Mach number
M_n	Mach number normal to wing leading edge
p	Static pressure
Re_c	Reynolds number based on wing chord
x	Distance from wing leading edge
α	Angle of incidence
φ	Angle of sweepback

REFERENCES

No.	*Author(s)*	*Title, etc.*
1	E. F. Lawlor	Wind tunnel tests at Mach numbers between 0·6 and 1·4 of a 60° swept wing having an aerofoil section designed for sub-critical flow at a Mach number of 1·2. Part I: 9% thick section with 'triangular' pressure distribution. A.R.C. C.P. 582 (1961).
2	—	Wing section design for two-dimensional tunnel tests. D.H. Aero Dept. A.90/PDJ (1958).
3	R. C. Pankhurst and H. B. Squire	Calculated pressure distributions for the R.A.E. 100–104 aerofoil sections. A.R.C. C.P. 80 (1950).
4	J. A. Bagley	Some aerodynamic principles for the design of swept wings. *Progress in Aeronautical Sciences* Vol. 3, Pergamon Press (1962).
5	J. Y. G. Evans	Transition fixing techniques and the interpretation of boundary layer conditions on slender wings in supersonic wind tunnels. R.A.E. Tech. Note Aero 2946 (A.R.C. 25892) (1964). (Also AIAA Aerodynamic Testing Conference Mach 9–10 1964).
6	Doris Cohen	Formulas for the supersonic loading, lift and drag of flat swept-back wings with leading edges behind the Mach lines. NACA Report 1050 (1951).
7	J. C. Cooke	The drag of infinite swept wings. A.R.C. C.P. 1040 (1964).
8	—	Royal Aeronautical Society Data Sheets, Vol. 2.

TABLE 1

Wing Section Ordinates.

(Normal to leading edge)

$\frac{x}{c}$	Upper surface $10^2 \frac{z}{c}$	Lower surface $-10^2 \frac{z}{c}$
0	0	0
0·001	0·442	0·412
0·002	0·663	0·573
0·003	0·783	0·693
0·004	0·912	0·792
0·005	1·026	0·878
0·010	1·486	1·198
0·02	2·156	1·614
0·03	2·679	1·909
0·04	3·119	2·145
0·06	3·844	2·516
0·08	4·437	2·807
0·10	4·944	3·042
0·15	5·971	3·451
0·2	6·760	3·688
0·25	7·353	3·825
0·3	7·780	3·884
0·35	8·058	3·874
0·4	8·188	3·808
0·45	8·161	3·687
0·5	7·955	3·497
0·55	7·527	3·198
0·574		3·034
0·6	6·943	
0·65	6·249	Straight
0·7	5·478	to
0·75	4·657	trailing
0·8	3·805	edge
0·85	2·925	
0·9	2·003	
0·95	1·030	
1·0	0	0

TABLE 2

Body Waisting.

Distance from wing root leading edge in	Semi-width of body	
	Upper surface in	Lower surface in
0*	2·4	2·4
0·25	2·382	2·384
0·5	2·358	2·368
1·0	2·300	2·330
2	2·126	2·247
3	1·928	2·158
4	1·711	2·067
5	1·500	1·970
6	1·316	1·876
7	1·163	1·786
8	1·063	1·704
9	1·018	1·633
10	1·018	1·582
11	1·058	1·551
12	1·121	1·544
13	1·209	1·554
14	1·319	1·577
14·86**	1·423	
15	1·435	1·611
16	1·519	1·649
17	1·605	1·691
18	1·691	1·742
19	1·773	1·804
20	1·860	1·874
21	1·940	1·947
22	2·025	2·025
23	2·102	
24	2·176	As
25	2·239	upper
26	2·290	surface
27	2·333	
28	2·368	
29	2·391	
30	2·400	2·400
Slope discontinuity in plan view:		
*Leading edge	0·06	0·06
**Trailing edge	0·045	0

TABLE 3a

Wing Pressure Coefficient.

$Re_c = 5{\cdot}73 \times 10^6$

α Degrees	−0·86	0	1·30	2·00	3·00
$\frac{x}{c}$%	Upper surface				
0·43	0·123	0·111	0·038	−0·022	−0·098
0·93	0·110	0·087	0·014	−0·042	−0·120
1·98	0·081	0·057	−0·015	−0·069	−0·140
3·00	0·064	0·036	−0·034	−0·081	−0·148
3·98	0·052	0·027	−0·044	−0·091	−0·149
7·98	0·023	−0·001	−0·050	−0·097	−0·157
9·93	0·010	−0·012	−0·057	−0·101	−0·168
14·88	−0·008	−0·026	−0·064	−0·103	−0·161
20·10	−0·017	−0·038	−0·073	−0·099	−0·154
25·11	−0·019	−0·050	−0·082	−0·097	−0·136
30·12	−0·038	−0·051	−0·090	−0·101	−0·124
35·10	−0·053	−0·058	−0·096	−0·108	−0·106
40·10	−0·064	−0·071	−0·085	−0·092	−0·103
45·10	−0·074	−0·085	−0·095	−0·096	−0·090
50·10	−0·066	−0·086	−0·099	−0·094	−0·073
55·10	−0·054	−0·062	−0·081	−0·075	−0·058
60·11	−0·046	−0·049	−0·059	−0·055	−0·049
65·11	−0·039	−0·040	−0·045	−0·043	−0·045
70·11	−0·030	−0·029	−0·033	−0·033	−0·042
75·12	−0·023		−0·027	−0·031	−0·042
80·13	−0·015	−0·015	−0·021	−0·027	−0·040
85·09	−0·009	−0·006	−0·014	−0·023	−0·036
90·10	−0·002	−0·000	−0·009	−0·021	−0·035
95·10	−0·000	0·002	−0·009	−0·021	−0·038
	Lower Surface				
0	0·059	0·103	0·123	0·102	0·059
0·48	−0·154	−0·050	0·066	0·103	0·131
3·74	−0·144	−0·052	0·015	0·048	0·090
5·96	−0·136	−0·052	0·003	0·031	0·069
9·96	−0·090	−0·051	−0·009	0·025	0·050
14·96	−0·067	−0·047	−0·007	0·024	0·042
19·96	−0·066	−0·046	−0·002	0·012	0·028
29·96	−0·054	−0·030	−0·011	−0·000	0·017
39·96	−0·046	−0·034	−0·017	−0·002	0·012
49·96	−0·041	−0·031	−0·016	−0·006	0·004
59·96	−0·026	−0·018	−0·009	−0·002	0·005
74·96	−0·012	−0·007	−0·005	−0·002	0·000
89·07	0·000	0·002	−0·003	−0·007	−0·013

TABLE 3b

$Re_c = 2{\cdot}86 \times 10^6$

α Degrees	−0·86	0	1·30	2·00	3·00
$\frac{x}{c}\%$	Upper surface				
0·43	0·129	0·113	0·046	−0·021	−0·098
0·93	0·114	0·090	0·020	−0·043	−0·120
1·98	0·086	0·059	−0·010	−0·070	−0·140
3·00	0·069	0·039	−0·028	−0·083	−0·149
3·98	0·059	0·029	−0·036	−0·091	−0·150
7·98	0·027	0·003	−0·048	−0·102	−0·158
9·93	0·016	−0·008	−0·053	−0·104	−0·166
14·88	−0·003	−0·022	−0·061	−0·103	−0·162
20·10	−0·015	−0·037	−0·068	−0·101	−0·153
25·11	−0·020	−0·049	−0·074	−0·102	−0·147
30·12	−0·037	−0·053	−0·085	−0·104	−0·145
35·10	−0·050	−0·061	−0·091	−0·111	−0·141
40·10	−0·058	−0·071	−0·087	−0·110	−0·137
45·10	−0·061	−0·078	−0·091	−0·105	−0·132
50·10	−0·056	−0·071	−0·095	−0·102	−0·120
55·10	−0·048	−0·056	−0·075	−0·096	−0·093
60·11	−0·040	−0·045	−0·055	−0·084	−0·065
65·11	−0·033	−0·036	−0·042	−0·056	−0·051
70·11	−0·024	−0·026	−0·029	−0·032	−0·038
75·12	−0·019		−0·020	−0·022	−0·029
80·13	−0·012	−0·014	−0·012	−0·015	−0·024
85·09	−0·007	−0·007	−0·007	−0·012	−0·018
90·10	−0·000	−0·000	−0·002	−0·008	−0·013
95·10	0·004	0·003	0·001	−0·009	−0·012
	Lower Surface				
0·00	0·067	0·106	0·130	0·102	0·059
0·48	−0·140	−0·043	0·075	0·108	0·137
3·74	−0·117	−0·055	0·022	0·051	0·087
5·96	−0·114	−0·054	0·014	0·039	0·068
9·96	−0·099	−0·050	0·007	0·031	0·052
14·96	−0·086	−0·041	0·005	0·022	0·039
19·96	−0·063	−0·038	0·005	0·012	0·029
29·96	−0·043	−0·027	−0·005	0·002	0·022
39·96	−0·038	−0·030	−0·007	0·001	0·015
49·96	−0·035	−0·026	−0·008	−0·004	0·006
59·96	−0·020	−0·013	0·000	0·002	0·009
74·96	−0·008	−0·005	0·003	0·001	0·005
89·07	0·001	0·002	0·004	−0·002	−0·002

TABLE 3c

$Re_c = 1{\cdot}44 \times 10^6$

α Degrees	0	1·30	2·00	3·00
$\frac{x}{c}\%$	Upper surface			
0·43	0·121	0·063	−0·007	−0·081
0·93	0·098	0·035	−0·031	−0·103
1·98	0·067	0·004	−0·057	−0·124
3·00	0·047	−0·012	−0·070	−0·133
3·98	0·038	−0·020	−0·078	−0·137
7·98	0·012	−0·037	−0·089	−0·146
9·93	0·000	−0·042	−0·091	−0·144
14·83	−0·012	−0·051	−0·091	−0·132
20·10	−0·028	−0·057	−0·086	−0·124
25·11	−0·039	−0·061	−0·084	−0·118
30·12	−0·050	−0·064	−0·082	−0·118
35·10	−0·057	−0·060	−0·078	−0·115
40·10	−0·065	−0·055	−0·072	−0·112
45·10	−0·070	−0·054	−0·070	−0·113
50·10	−0·068	−0·050	−0·071	−0·112
55·10	−0·061	−0·050	−0·069	−1·101
60·11	−0·052	−0·047	−0·067	−0·090
65·11	−0·037	−0·050	−0·069	−0·087
70·11	−0·018	−0·047	−0·067	−0·070
75·12		−0·047	−0·069	−0·047
80·13	−0·007	−0·042	−0·066	−0·033
85·09	0·001	−0·034	−0·056	−0·020
90·10	0·012	−0·018	−0·039	−0·012
95·10	0·016	−0·005	−0·026	−0·005
	Lower surface			
0·00	0·117	0·142	0·111	0·072
0·48	−0·030	0·085	0·117	0·145
3·74	−0·047	0·031	0·060	0·095
5·96	−0·047	0·024	0·048	0·078
9·96	−0·043	0·015	0·037	0·061
14·96	−0·034	0·013	0·025	0·047
19·96	−0·032	0·010	0·020	0·039
29·96	−0·023	0·005	0·010	0·033
39·96	−0·021	0·004	0·010	0·026
49·96	−0·019	0·001	0·005	0·019
59·96	−0·004	0·008	0·012	0·024
74·96	0·011	0·009	0·010	0·017
89·07	0·015	0·009	0·003	0·006

TABLE 4a

$$Wing \frac{p}{H_n}$$

$$Re_c = 5{\cdot}73 \times 10^6$$

α Degrees	−0·86	0	1·30	2·00	3·00
$\frac{x}{c}\%$	Upper surface				
0·43	0·9834	0·9587	0·8085	0·6861	0·5293
0·93	0·9556	0·9094	0·7599	0·6434	0·4848
1·98	0·8961	0·8474	0·6988	0·5887	0·4431
3·00	0·8606	0·8049	0·6599	0·5638	0·4258
3·98	0·8362	0·7854	0·6403	0·5441	0·4235
7·98	0·7772	0·7289	0·6280	0·5302	0·4072
9·93	0·7509	0·7065	0·6125	0·5230	0·3852
14·88	0·7131	0·6761	0·5995	0·5197	0·4004
20·10	0·6947	0·6518	0·5813	0·5278	0·4149
25·11	0·6918	0·6279	0·5618	0·5322	0·4507
30·12	0·6521	0·6256	0·5455	0·5240	0·4767
35·10	0·6214	0·6109	0·5323	0·5081	0·5120
40·10	0·5984	0·5838	0·5550	0·5417	0·5183
45·10	0·5786	0·5553	0·5346	0·5331	0·5456
50·10	0·5959	0·5540	0·5263	0·5384	0·5796
55·10	0·6185	0·6036	0·5646	0·5772	0·6113
60·11	0·6366	0·6291	0·6100	0·6176	0·6304
65·11	0·6506	0·6483	0·6371	0·6415	0·6380
70·11	0·6697	0·6701	0·6616	0·6617	0·6443
75·12	0·6822		0·6746	0·6669	0·6438
80·13	0·6995	0·6994	0·6882	0·6742	0·6477
85·09	0·7129	0·7173	0·7020	0·6823	0·6563
90·10	0·7269	0·7298	0·7122	0·6875	0·6592
95·10	0·7298	0·7343	0·7112	0·6866	0·6515
	Lower surface				
0	0·8520	0·9417	0·9829	0·9394	0·8512
0·48	0·4138	0·6283	0·8661	0·9422	0·9987
3·74	0·4355	0·6235	0·7603	0·8277	0·9159
5·96	0·4518	0·6245	0·7368	0·7946	0·8719
9·96	0·5458	0·6251	0·7126	0·7806	0·8326
14·96	0·5937	0·6331	0·7161	0·7792	0·8154
19·96	0·5956	0·6350	0·7259	0·7553	0·7886
29·96	0·6200	0·6683	0·7077	0·7299	0·7655
39·96	0·6369	0·6609	0·6949	0·7255	0·7545
49·96	0·6464	0·6670	0·6985	0·7174	0·7378
59·96	0·6775	0·6938	0·7115	0·7255	0·7397
74·96	0·7053	0·7155	0·7209	0·7265	0·7311
89·07	0·7303	0·7337	0·7241	0·7150	0·7043

TABLE 4b

$Re_c = 2{\cdot}86 \times 10^6$

α Degrees	−0·86	0	1·30	2·00	3·00
$\frac{x}{c}\%$	Upper surface				
0·43	0·9943	0·9620	0·8252	0·6877	0·5296
0·93	0·9638	0·9150	0·7718	0·6424	0·4864
1·98	0·9066	0·8512	0·7099	0·5870	0·4456
3·00	0·8723	0·8099	0·6743	0·5603	0·4265
3·98	0·8509	0·7904	0·6585	0·5444	0·4234
7·98	0·7865	0·7369	0·6337	0·5221	0·4082
9·93	0·7632	0·7155	0·6224	0·5177	0·3910
14·88	0·7250	0·6853	0·6059	0·5202	0·3990
20·10	0·7007	0·6562	0·5926	0·5253	0·4177
25·11	0·6912	0·6314	0·5787	0·5229	0·4303
30·12	0·6545	0·6227	0·5578	0·5177	0·4337
35·10	0·6298	0·6070	0·5453	0·5049	0·4418
40·10	0·6126	0·5855	0·5521	0·5068	0·4502
45·10	0·6054	0·5706	0·5439	0·5163	0·4609
50·10	0·6169	0·5868	0·5369	0·5215	0·4845
55·10	0·6336	0·6169	0·5768	0·5354	0·5418
60·11	0·6497	0·6394	0·6192	0·5592	0·5972
65·11	0·6645	0·6566	0·6447	0·6176	0·6262
70·11	0·6817	0·6773	0·6726	0·6661	0·6537
75·12	0·6931		0·6901	0·6858	0·6716
80·13	0·7065	0·7029	0·7061	0·7005	0·6831
85·09	0·7160	0·7159	0·7162	0·7068	0·6945
90·10	0·7308	0·7312	0·7270	0·7150	0·7041
95·10	0·7384	0·7377	0·7327	0·7131	0·7060
	Lower surface				
0·00	0·8685	0·9471	0·9982	0·9398	0·8522
0·48	0·4436	0·6434	0·8842	0·9513	
3·74	0·4908	0·6186	0·7753	0·8362	0·9083
5·96	0·4984	0·6205	0·7588	0·8100	0·8702
9·96	0·5289	0·6289	0·7447	0·7953	0·8377
14·96	0·5556	0·6472	0·7423	0·7756	0·8110
19·96	0·6013	0·6529	0·7411	0·7546	0·7900
29·96	0·6437	0·6755	0·7202	0·7350	0·7752
39·96	0·6528	0·6701	0·7177	0·7336	0·7626
49·96	0·6604	0·6782	0·7151	0·7227	0·7442
59·96	0·6894	0·7049	0·7316	0·7355	0·7500
74·96	0·7142	0·7217	0·7366	0·7336	0·7404
89·07	0·7332	0·7351	0·7391	0·7279	0·7271

TABLE 4c

$Re_c = 1{\cdot}44 \times 10^6$

α Degrees	0	1·30	2·00	3·00
$\frac{x}{c}\%$	Upper surface			
0·43	0·9799	0·8613	0·7169	0·5663
0·93	0·9314	0·8027	0·6681	0·5214
1·98	0·8696	0·7407	0·6148	0·4790
3·00	0·8287	0·7073	0·5882	0·4600
3·98	0·8092	0·6914	0·5723	0·4531
7·98	0·7560	0·6556	0·5501	0·4342
9·93	0·7327	0·6459	0·5457	0·4379
14·88	0·7066	0·6276	0·5463	0·4632
20·10	0·6757	0·6163	0·5571	0·4797
25·11	0·6529	0·6080	0·5603	0·4904
30·12	0·6310	0·6004	0·5647	0·4917
35·10	0·6153	0·6104	0·5730	0·4980
40·10	0·5996	0·6194	0·5844	0·5024
45·10	0·5887	0·6225	0·5882	0·5018
50·10	0·5934	0·6307	0·5875	0·5024
55·10	0·6082	0·6307	0·5920	0·5252
60·11	0·6267	0·6352	0·5945	0·5480
65·11	0·6571	0·6300	0·5920	0·5542
70·11	0·6947	0·6369	0·5945	0·5890
75·12		0·6359	0·5913	0·6352
80·13	0·7184	0·6459	0·5983	0·6656
85·09	0·7332	0·6618	0·6180	0·6921
90·10	0·7560	0·6952	0·6528	0·7073
95·10	0·7645	0·7217	0·6795	0·7225
	Lower surface			
0·00	0·9708		0·9584	0·8793
0·48	0·6705	0·9050	0·9698	
3·74	0·6363	0·7943	0·8551	0·9254
5·96	0·6363	0·7799	0·8291	0·8913
9·96	0·6449	0·7623	0·8069	0·8572
14·96	0·6629	0·7578	0·7835	0·8268
19·96	0·6667	0·7527	0·7721	0·8117
29·96	0·6853	0·7413	0·7524	0·7990
39·96	0·6896	0·7406	0·7531	0·7845
49·96	0·6938	0·7344	0·7423	0·7700
59·96	0·7242	0·7489	0·7569	0·7813
74·96	0·7542	0·7503	0·7531	0·7662
89·07	0·7618	0·7510	0·7379	0·7434

TABLE 5a

Wing Mach Number.

$Re_c = 5{\cdot}73 \times 10^6$

α Degrees	−0·86	0	1·30	2·00	3·00
$\frac{x}{c}\%$	Upper surface				
0·43	1·812	1·829	1·939	2·044	2·210
0·93	1·831	1·863	1·979	2·085	2·266
1·98	1·872	1·909	2·032	2·142	2·324
3·00	1·899	1·942	2·069	2·170	2·349
3·98	1·917	1·957	2·088	2·193	2·353
7·98	1·964	2·005	2·101	2·209	2·378
9·93	1·986	2·025	2·117	2·218	2·413
14·88	2·019	2·054	2·131	2·222	2·389
20·10	2·036	2·077	2·150	2·212	2·366
25·11	2·039	2·101	2·172	2·207	2·313
30·12	2·077	2·103	2·191	2·217	2·277
35·10	2·108	2·119	2·207	2·236	2·231
40·10	2·132	2·148	2·180	2·195	2·224
45·10	2·153	2·180	2·204	2·206	2·191
50·10	2·134	2·181	2·214	2·199	2·152
55·10	2·111	2·126	2·169	2·155	2·118
60·11	2·092	2·100	2·119	2·112	2·098
65·11	2·078	2·080	2·092	2·087	2·091
70·11	2·060	2·059	2·067	2·067	2·085
75·12	2·048		2·055	2·062	2·085
80·13	2·032	2·032	2·042	2·055	2·081
85·09	2·020	2·016	2·029	2·048	2·073
90·10	2·007	2·005	2·020	2·043	2·070
95·10	2·005	2·001	2·021	2·044	2·077
	Lower surface				
0	1·905	1·840	1·812	1·842	1·906
0·48	2·367	2·101	1·894	1·840	1·802
3·74	2·335	2·105	1·978	1·924	1·858
5·96	2·311	2·104	1·999	1·950	1·890
9·96	2·191	2·104	2·020	1·961	1·920
14·96	2·137	2·096	2·017	1·963	1·933
19·96	2·135	2·094	2·008	1·983	1·955
29·96	2·109	2·061	2·024	2·005	1·974
39·96	2·092	2·068	2·036	2·008	1·983
49·96	2·082	2·062	2·033	2·016	1·998
59·96	2·052	2·037	2·021	2·008	1·996
74·96	2·026	2·017	2·013	2·008	2·003
89·07	2·004	2·001	2·010	2·018	2·027

TABLE 5b

$Re_c = 2{\cdot}86 \times 10^6$

α Degrees	−0·86	0	1·30	2·00	3·00
$\frac{x}{c}\%$	Upper surface				
0·43	1·801	1·823	1·922	2·039	2·207
0·93	1·822	1·856	1·965	2·083	2·261
1·98	1·862	1·902	2·019	2·141	2·317
3·00	1·887	1·934	2·052	2·171	2·345
3·98	1·903	1·950	2·067	2·189	2·350
7·98	1·953	1·995	2·092	2·216	2·373
9·93	1·973	2·014	2·103	2·221	2·401
14·88	2·006	2·042	2·121	2·218	2·388
20·10	2·027	2·069	2·135	2·212	2·358
25·11	2·036	2·094	2·150	2·215	2·339
30·12	2·071	2·103	2·173	2·221	2·334
35·10	2·096	2·119	2·188	2·237	2·322
40·10	2·114	2·142	2·180	2·235	2·310
45·10	2·121	2·159	2·190	2·223	2·295
50·10	2·109	2·141	2·198	2·216	2·263
55·10	2·092	2·109	2·152	2·200	2·192
60·11	2·076	2·086	2·107	2·172	2·130
65·11	2·061	2·069	2·081	2·108	2·099
70·11	2·045	2·049	2·054	2·060	2·072
75·12	2·034		2·037	2·041	2·055
80·13	2·022	2·025	2·023	2·028	2·044
85·09	2·014	2·014	2·013	2·022	2·033
90·10	2·001	2·000	2·004	2·015	2·024
95·10	1·994	1·994	1·999	2·016	2·023
	Lower surface				
0·00	1·889	1·833	1·799	1·838	1·902
0·48	2·320	2·082	1·878	1·830	1·791
3·74	2·255	2·107	1·963	1·914	1·860
5·96	2·245	2·105	1·976	1·934	1·888
9·96	2·207	2·097	1·988	1·946	1·913
14·96	2·176	2·078	1·991	1·962	1·934
19·96	2·125	2·073	1·992	1·980	1·950
29·96	2·082	2·051	2·010	1·997	1·963
39·96	2·073	2·056	2·012	1·998	1·973
49·96	2·065	2·048	2·014	2·008	1·989
59·96	2·038	2·024	2·000	1·996	1·984
74·96	2·015	2·009	1·995	1·998	1·992
89·07	1·998	1·997	1·993	2·003	2·004

TABLE 5c

$Re_c = 1{\cdot}44 \times 10^6$

α Degrees	0	1·30	2·00	3·00
$\frac{x}{c}$ – %	Upper surface			
0·43	1·808	1·891	2·010	2·161
0·93	1·841	1·937	2·055	2·213
1·98	1·885	1·989	2·108	2·267
3·00	1·916	2·018	2·136	2·293
3·98	1·932	2·033	2·154	2·303
7·98	1·975	2·067	2·179	2·330
9·93	1·996	2·076	2·184	2·325
14·88	2·019	2·095	2·183	2·289
20·10	2·047	2·106	2·171	2·267
25·11	2·069	2·115	2·167	2·252
30·12	2·091	2·123	2·162	2·251
35·10	2·107	2·113	2·153	2·243
40·10	2·124	2·103	2·140	2·237
45·10	2·136	2·100	2·136	2·238
50·10	2·131	2·092	2·137	2·237
55·10	2·115	2·092	2·132	2·209
60·11	2·096	2·087	2·129	2·182
65·11	2·065	2·092	2·132	2·174
70·11	2·030	2·085	2·129	2·135
75·12		2·086	2·133	2·087
80·13	2·008	2·076	2·125	2·057
85·09	1·995	2·061	2·105	2·032
90·10	1·975	2·029	2·070	2·018
95·10	1·968	2·005	2·044	2·005
	Lower surface			
0·00	1·814	1·780	1·822	1·878
0·48	2·052	1·859	1·814	1·777
3·74	2·086	1·944	1·896	1·845
5·96	2·086	1·956	1·916	1·869
9·96	2·077	1·970	1·934	1·895
14·96	2·060	1·974	1·953	1·918
19·96	2·056	1·978	1·962	1·930
29·96	2·038	1·988	1·979	1·940
39·96	2·034	1·989	1·978	1·952
49·96	2·031	1·994	1·987	1·964
59·96	2·003	1·982	1·975	1·954
74·96	1·977	1·980	1·978	1·967
89·07	1·971	1·980	1·991	1·986

TABLE 6a

Wing Body Junction Pressure Coefficient.

$Re_c = 5{\cdot}73 \times 10^6$

α Degrees	−0·86	0	1·30	2·00	3·00
$\frac{x}{c}\%$	Upper surface				
0·5		0·027	0·019		−0·016
1·0	0·028	0·031	0·020	0·007	−0·009
2·0	0·027	0·016	−0·000	−0·014	−0·031
4·0	0·005	−0·008	−0·027	−0·040	−0·058
6·0	−0·008	−0·024	−0·043	−0·055	−0·076
10·0	−0·041	−0·052	−0·075	−0·088	−0·106
15·0	−0·051	−0·063	−0·085	−0·097	−0·115
20·0	−0·038	−0·050	−0·070	−0·080	−0·096
30·0		−0·037			
40·0	−0·010	−0·018	−0·028	−0·033	−0·041
50·0	0·007	−0·003	−0·013	−0·023	−0·028
60·0	0·032	0·023	0·006	−0·001	−0·010
75·0	0·069	0·055	0·033	0·025	0·013
90·0	0·007	0·071	0·048	0·038	0·022
100·0	0·046		0·029	0·024	0·014
	Lower surface				
0·5	0·041	0·049	0·056	0·056	0·054
1·0	0·002	0·024	0·028	0·035	0·037
2·0	−0·020	−0·002	0·008	0·017	0·027
4·0	−0·039	−0·002	−0·006	0·005	0·021
6·0	−0·040	−0·022	−0·004	0·008	0·025
10·0	−0·046	−0·027	−0·007	0·005	0·022
15·0	−0·045	−0·030	−0·008	0·004	0·019
20·0	−0·048	−0·031	−0·012	−0·002	0·012
30·0	−0·034	−0·020	−0·003	0·007	0·021
40·0	−0·026	−0·013	0·000	0·010	0·020
50·0	−0·021	−0·010	0·002	0·011	0·021
60·0	−0·018	−0·009	0·004	0·012	0·021
75·0	0·009	0·019	0·031	0·039	0·048

TABLE 6b

$Re_c = 2{\cdot}86 \times 10^6$

α Degrees	−0·86	0	1·30	2·00	3·00
$\frac{x}{c}$ %	Upper surface				
0·5	0·031	0·029	0·029	0·011	−0·002
1·0	0·033	0·030	0·024	0·009	−0·004
2·0	0·023	0·009	0·004	−0·011	−0·028
4·0	−0·000	−0·012	−0·024	−0·042	−0·061
6·0	−0·012	−0·025	−0·039	−0·057	−0·076
10·0	−0·036	−0·047	−0·065	−0·083	−0·099
15·0	−0·045	−0·056	−0·074	−0·090	−0·106
20·0	−0·033	−0·044	−0·060	−0·075	−0·088
30·0		−0·035			
40·0	−0·007	−0·017	−0·021	−0·033	−0·039
50·0	0·002	−0·003	−0·012	−0·023	−0·032
60·0	0·025	0·017	0·007	−0·005	−0·013
75·0	0·066	0·053	0·037	0·023	0·010
90·0	0·078	0·066	0·048	0·032	0·018
100·0	0·049		0·024	0·011	0·003
	Lower surface				
0·5	0·036	0·040	0·048	0·046	0·044
1·0	0·010	0·026	0·035	0·036	0·039
2·0	−0·018	−0·005	0·007	0·010	0·021
4·0	−0·038	0·019	−0·003	0·001	0·019
6·0	−0·039	−0·023	−0·002	0·006	0·020
10·0	−0·042	−0·026	−0·003	0·005	0·019
15·0	−0·039	−0·027	−0·002	0·005	0·019
20·0	−0·040	−0·027	−0·005	0·000	0·013
30·0	−0·029	−0·015	0·003	0·008	0·020
40·0	−0·023	−0·012	0·004	0·008	0·020
50·0	−0·018	−0·009	0·007	0·010	0·020
60·0	−0·014	−0·007	0·010	0·012	0·023
75·0	0·013	0·021	0·038	0·040	0·051
90·0	0·024	0·034	0·052	0·055	0·066

TABLE 6c

$Re_c = 1{\cdot}44 \times 10^6$

α Degrees	0	1·30	2·00	3·00
$\frac{x}{c}\%$	Upper surface			
0·5	0·028	0·031	0·017	0·009
1·0	0·031	0·027	0·016	0·006
2·0	0·017	0·005	−0·008	−0·019
4·0	−0·000	−0·014	−0·034	−0·046
6·0	−0·014	−0·028	−0·048	−0·062
10·0	−0·034	−0·054	−0·072	−0·086
15·0	−0·045	−0·062	−0·079	−0·093
20·0	−0·032	−0·049	−0·066	−0·075
30·0	−0·021			
40·0	−0·006	−0·010	−0·024	−0·030
50·0	0·006	−0·007	−0·020	−0·025
60·0	0·021	0·011	−0·002	−0·009
75·0	0·058	0·044	0·029	0·019
90·0	0·067	0·050	0·035	0·024
100·0		0·031	0·014	0·006
	Lower surface			
0·5	0·041	0·048	0·042	0·041
1·0	0·037	0·047	0·044	0·050
2·0	−0·005	0·009	0·007	0·022
4·0		−0·000	0·003	0·021
6·0	−0·017	0·003	0·008	0·025
10·0	−0·017	0·005	0·010	0·026
15·0	−0·015	0·007	0·011	0·026
20·0	−0·017	0·005	0·009	0·022
30·0	−0·008	0·008	0·012	0·026
40·0	−0·005	0·011	0·014	0·028
50·0	−0·002	0·015	0·016	0·008
60·0	−0·000	0·016	0·018	0·030
75·0	0·026	0·046	0·048	0·060
90·0	0·039	0·058	0·059	0·073

TABLE 7a

Wing Body Junction $\frac{p}{H_n}$

$Re_c = 5{\cdot}73 \times 10^6$

α Degrees	−0·86	0	1·30	2·00	3·00
$\frac{x}{c}\%$	Upper surface				
0·5		0·7864	0·7688		0·6976
1·0	0·7878	0·7938	0·7703	0·7443	0·7120
2·0	0·7860	0·7625	0·7295	0·7006	0·6660
4·0	0·7414	0·7130	0·6751	0·6488	0·6104
6·0	0·7145	0·6817	0·6428	0·6167	0·5735
10·0	0·6463	0·6242	0·5767	0·5506	0·5132
15·0	0·6257	0·6015	0·5558	0·5309	0·4936
20·0	0·6526	0·6274	0·5874	0·5654	0·5343
30·0		0·6539			
40·0	0·7101	0·6925	0·6736	0·6618	0·6468
50·0	0·7442	0·7235	0·7044	0·6833	0·6738
60·0	0·7949	0·7778	0·7433	0·7293	0·7100
75·0	0·8722	0·8433	0·7975	0·7816	0·7560
90·0	0·8875	0·8756	0·8278	0·8075	0·7760
100·0	0·8252		0·7889	0·7792	0·7598
	Lower surface				
0·5	0·8152	0·8308	0·8450	0·8454	0·8403
1·0	0·7341	0·7788	0·7881	0·8022	0·8062
2·0	0·6900	0·7267	0·7467	0·7648	0·7851
4·0	0·6501	0·7265	0·7171	0·7409	0·7742
6·0	0·6484	0·6842	0·7224	0·7471	0·7824
10·0	0·6353	0·6759	0·7153	0·7409	0·7752
15·0	0·6388	0·6679	0·7138	0·7385	0·7685
20·0	0·6321	0·6657	0·7048	0·7265	0·7550
30·0	0·6614	0·6897	0·7240	0·7443	0·7738
40·0	0·6766	0·7031	0·7310	0·7500	0·7717
50·0	0·6867	0·7091	0·7352	0·7533	0·7742
60·0	0·6929	0·7127	0·7383	0·7539	0·7723
75·0	0·7490	0·7688	0·7942	0·8109	0·8293
90·0	0·7793	0·8011	0·8322	0·8483	0·8680

TABLE 7b

$Re_c = 2{\cdot}86 \times 10^6$

α Degrees	−0·86	0	1·30	2·00	3·00
$\frac{x}{c}\%$	Upper surface				
0·5	0·7938	0·7898	0·7898	0·7538	0·7271
1·0	0·7980	0·7920	0·7797	0·7503	0·7232
2·0	0·7781	0·7485	0·7385	0·7088	0·6736
4·0	0·7309	0·7968	0·6822	0·6458	0·6068
6·0	0·7061	0·6793	0·6506	0·6147	0·5755
10·0	0·6575	0·6354	0·5985	0·5612	0·5278
15·0	0·6399	0·6166	0·5802	0·5465	0·5133
20·0	0·6646	0·6415	0·6087	0·5771	0·5507
30·0		0·6602			
40·0	0·7161	0·6969	0·6885	0·6643	0·6507
50·0	0·7347	0·7259	0·7073	0·6840	0·6656
60·0	0·7832	0·7650	0·7447	0·7214	0·7042
75·0	0·8666	0·8386	0·8069	0·7781	0·7519
90·0	0·8914	0·8669	0·8291	0·7972	0·7675
100·0	0·8304		0·7803	0·7527	0·7366
	Lower surface				
0·5	0·8052	0·8138	0·8291	0·8253	0·8206
1·0	0·7523	0·7848	0·8019	0·8043	0·8103
2·0	0·6951	0·7206	0·7461	0·7519	0·7740
4·0	0·6537	0·7706	0·7252	0·7336	0·7690
6·0	0·6508	0·6839	0·7265	0·7426	0·7717
10·0	0·6456	0·6786	0·7259	0·7413	0·7709
15·0	0·6508	0·6763	0·7265	0·7418	0·7690
20·0	0·6489	0·6759	0·7202	0·7317	0·7576
30·0	0·6714	0·7007	0·7373	0·7464	0·7717
40·0	0·6837	0·7071	0·7398	0·7484	0·7721
50·0	0·6947	0·7126	0·7461	0·7508	0·7729
60·0	0·7028	0·7179	0·7525	0·7560	0·7786
75·0	0·7576	0·7741	0·8082	0·8138	0·8347
90·0	0·7800	0·8004	0·8380	0·8444	0·8664

TABLE 7c

$Re_c = 1{\cdot}44 \times 10^6$

α Degrees	0	1·30	2·00	3·00
$\frac{x}{c}\%$	Upper surface			
0·5	0·7898	0·7957	0·7657	0·7510
1·0	0·7955	0·7875	0·7638	0·7434
2·0	0·7656	0·7427	0·7150	0·6941
4·0	0·7318	0·7034	0·6618	0·6372
6·0	0·7043	0·6755	0·6346	0·6062
10·0	0·6625	0·6221	0·5851	0·5569
15·0	0·6401	0·6055	0·5706	0·5424
20·0	0·6667	0·6321	0·5972	0·5797
30·0	0·6891			
40·0	0·7200	0·7117	0·6840	0·6714
50·0	0·7432	0·7175	0·6922	0·6803
50·0	0·7746	0·7547	0·7277	0·7131
75·0	0·8497	0·8223	0·7917	0·7700
90·0	0·8682	0·8329	0·8031	0·7800
100·0		0·7957	0·7607	0·7434
	Lower surface			
0·5	0·8155	0·8292	0·8177	0·8155
1·0	0·8074	0·8285	0·8215	0·8337
2·0	0·7209	0·7503	0·7467	0·7769
4·0		0·7313	0·7379	0·7737
6·0	0·6976	0·7382	0·7486	0·7820
10·0	0·6981	0·7413	0·7531	0·7851
15·0	0·7014	0·7458	0·7537	0·7851
20·0	0·6972	0·7413	0·7493	0·7775
30·0	0·7162	0·7489	0·7562	0·7858
40·0	0·7224	0·7534	0·7600	0·7882
50·0	0·7280	0·7616	0·7645	0·7472
60·0	0·7314	0·7640	0·7676	0·7927
75·0	0·7855	0·8254	0·8291	0·8540
90·0	0·8117	0·8512	0·8519	0·8799

TABLE 8a

Wing Body Junction Mach Number.

$Re_c = 5{\cdot}73 \times 10^6$

α Degrees	−0·86	0	1·30	2·00	3·00
$\frac{x}{c}\%$	Upper surface				
0·5		1·957	1·971		2·034
1·0	1·956	1·951	1·970	1·992	2·020
2·0	1·957	1·977	2·005	2·031	2·063
4·0	1·995	2·020	2·054	2·080	2·119
6·0	2·018	2·048	2·086	2·112	2·159
10·0	2·082	2·105	2·155	2·185	2·230
15·0	2·103	2·128	2·179	2·208	2·255
20·0	2·076	2·102	2·144	2·168	2·204
30·0		2·075			
40·0	2·022	2·038	2·056	2·067	2·082
50·0	1·992	2·010	2·027	2·047	2·056
60·0	1·950	1·964	1·993	2·005	2·022
75·0	1·890	1·912	1·948	1·961	1·982
90·0	1·879	1·887	1·924	1·940	1·965
100·0	1·926		1·955	1·963	1·979
	Lower surface				
0·5	1·934	1·921	1·910	1·910	1·914
1·0	2·001	1·963	1·955	1·944	1·941
2·0	2·041	2·007	1·990	1·975	1·958
4·0	2·079	2·008	2·016	1·995	1·967
6·0	2·080	2·046	2·011	1·990	1·960
10·0	2·093	2·054	2·017	1·995	1·966
15·0	2·090	2·061	2·019	1·997	1·972
20·0	2·097	2·064	2·027	2·008	1·983
30·0	2·068	2·041	2·010	1·992	1·967
40·0	2·053	2·028	2·004	1·987	1·969
50·0	2·044	2·023	2·000	1·984	1·967
60·0	2·038	2·020	1·997	1·984	1·968
75·0	1·988	1·971	1·950	1·937	1·922
90·0	1·962	1·945	1·920	1·908	1·893

TABLE 8b

$Re_c = 2{\cdot}86 \times 10^6$

α Degrees	−0·86	0	1·30	2·00	3·00
$\frac{x}{c}\%$	Upper surface				
0·5	1·947	1·951	1·951	1·981	2·004
1·0	1·944	1·949	1·959	1·984	2·007
2·0	1·960	1·985	1·994	2·020	2·053
4·0	2·000	2·022	2·045	2·080	2·120
6·0	2·023	2·047	2·075	2·111	2·153
10·0	2·068	2·090	2·128	2·170	2·209
15·0	2·086	2·109	2·148	2·187	2·227
20·0	2·061	2·084	2·118	2·152	2·182
30·0		2·066			
40·0	2·014	2·031	2·039	2·062	2·075
50·0	1·997	2·005	2·021	2·043	2·060
60·0	1·956	1·971	1·988	2·009	2·024
75·0	1·891	1·912	1·937	1·960	1·982
90·0	1·873	1·891	1·919	1·945	1·969
100·0	1·918		1·958	1·982	1·995
	Lower surface				
0·5	1·938	1·931	1·919	1·922	1·926
1·0	1·982	1·955	1·941	1·939	1·934
2·0	2·033	2·009	1·987	1·982	1·964
4·0	2·072	1·966	2·005	1·998	1·968
6·0	2·075	2·043	2·004	1·990	1·966
10·0	2·080	2·048	2·005	1·991	1·966
15·0	2·075	2·050	2·004	1·991	1·968
20·0	2·077	2·051	2·010	2·000	1·977
30·0	2·055	2·027	1·995	1·987	1·966
40·0	2·043	2·022	1·993	1·985	1·965
50·0	2·033	2·017	1·987	1·983	1·965
60·0	2·026	2·012	1·982	1·979	1·960
75·0	1·977	1·964	1·936	1·931	1·915
90·0	1·959	1·942	1·913	1·908	1·891

TABLE 8c

$Re_c = 1{\cdot}44 \times 10^6$

α Degrees	0	1·30	2·00	3·00
$\frac{x}{c}\%$	Upper surface			
0·5	1·947	1·943	1·967	1·980
1·0	1·943	1·949	1·969	1·986
2·0	1·967	1·987	2·011	2·030
4·0	1·996	2·022	2·061	2·085
6·0	2·021	2·048	2·088	2·117
10·0	2·060	2·100	2·140	2·171
15·0	2·082	2·118	2·156	2·188
20·0	2·056	2·090	2·127	2·146
30·0	2·035			
40·0	2·007	2·014	2·040	2·052
50·0	1·986	2·009	2·032	2·043
60·0	1·960	1·977	2·000	2·013
75·0	1·900	1·921	1·946	1·964
90·0	1·886	1·913	1·937	1·955
100·0		1·943	1·972	1·986
	Lower surface			
0·5	1·927	1·916	1·925	1·927
1·0	1·933	1·917	1·922	1·913
2·0	2·006	1·980	1·983	1·958
4·0		1·997	1·991	1·961
6·0	2·027	1·991	1·982	1·954
10·0	2·027	1·988	1·978	1·951
15·0	2·024	1·984	1·977	1·951
20·0	2·027	1·988	1·981	1·957
30·0	2·010	1·982	1·975	1·951
40·0	2·005	1·978	1·972	1·949
50·0	2·000	1·971	1·968	1·983
60·0	1·997	1·969	1·966	1·945
75·0	1·951	1·919	1·916	1·897
90·0	1·930	1·899	1·899	1·878

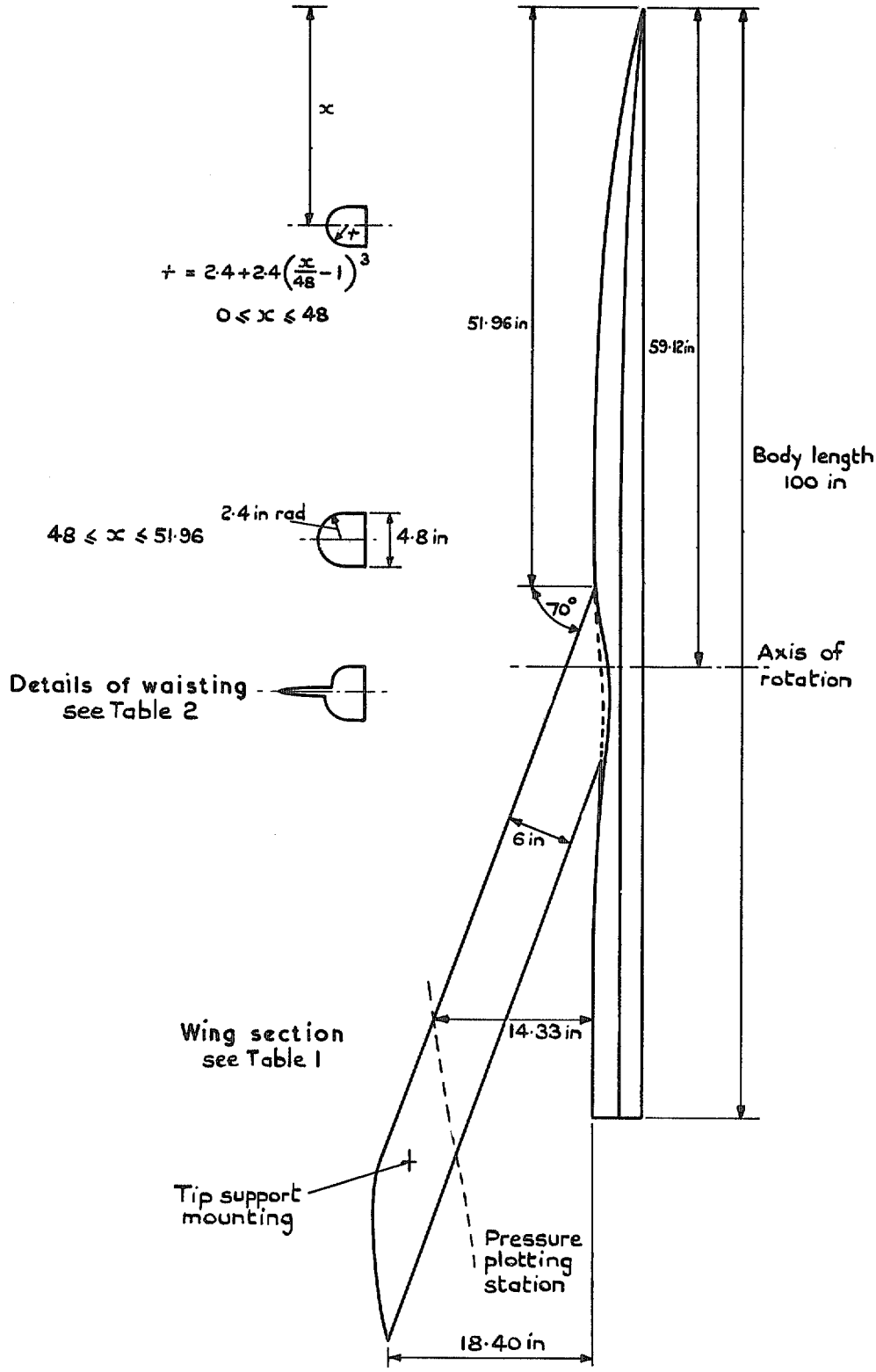

FIG. 1. Arrangement of model.

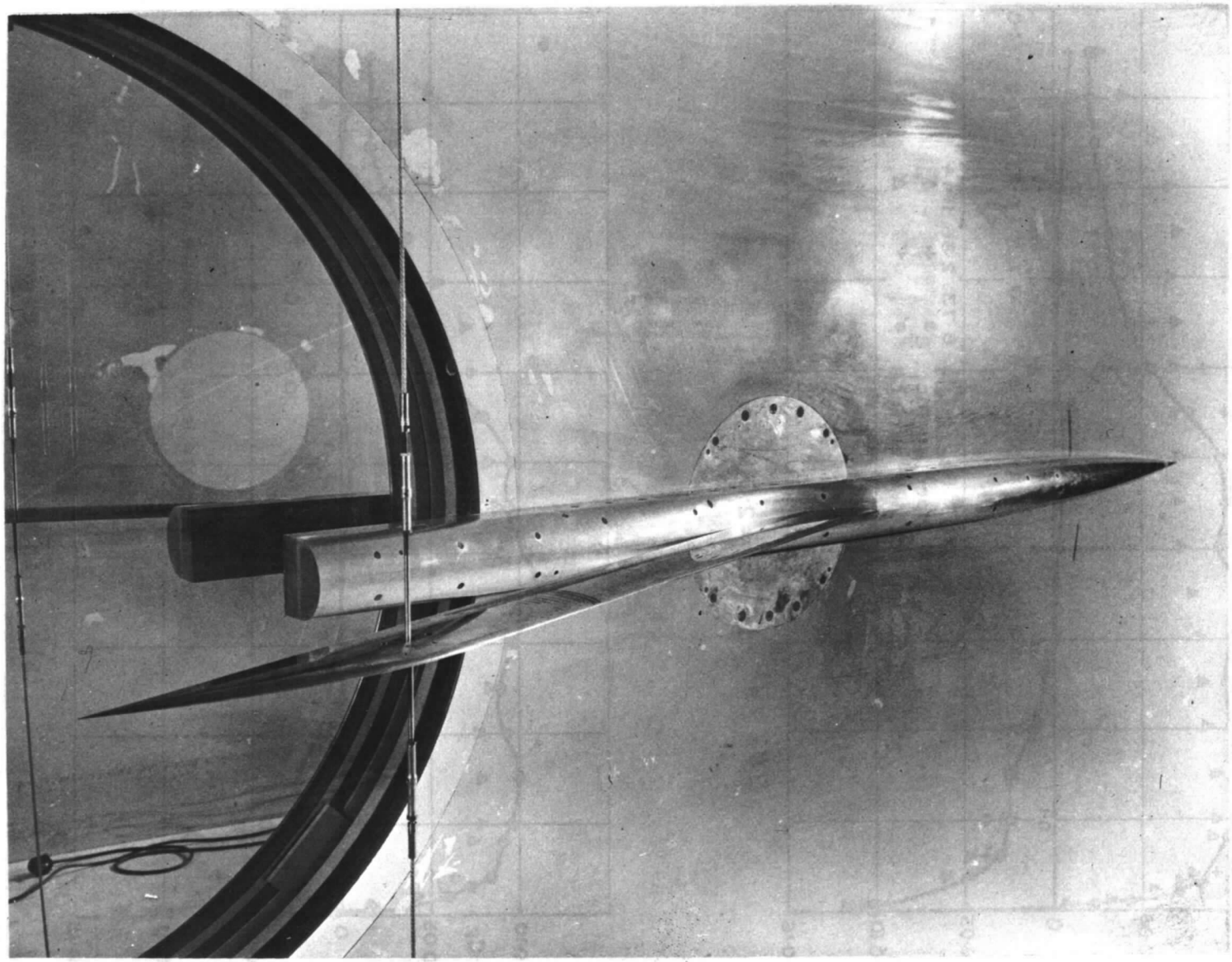

FIG. 2. Model mounted in tunnel.

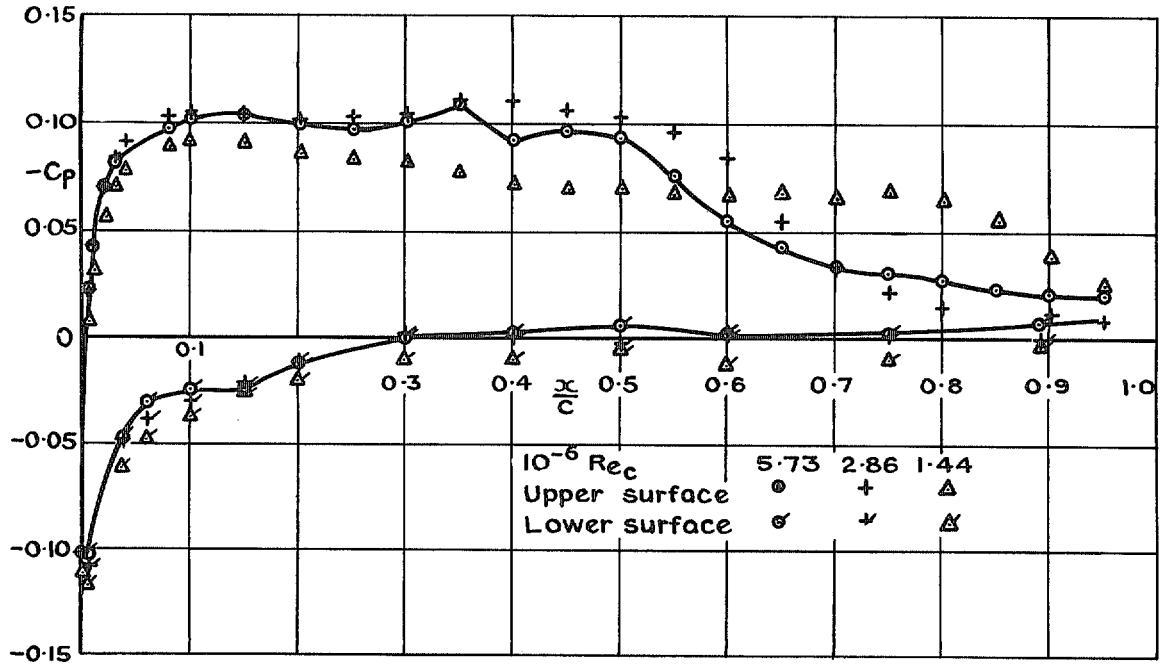

(a) $\alpha = 2{\cdot}0$ degrees

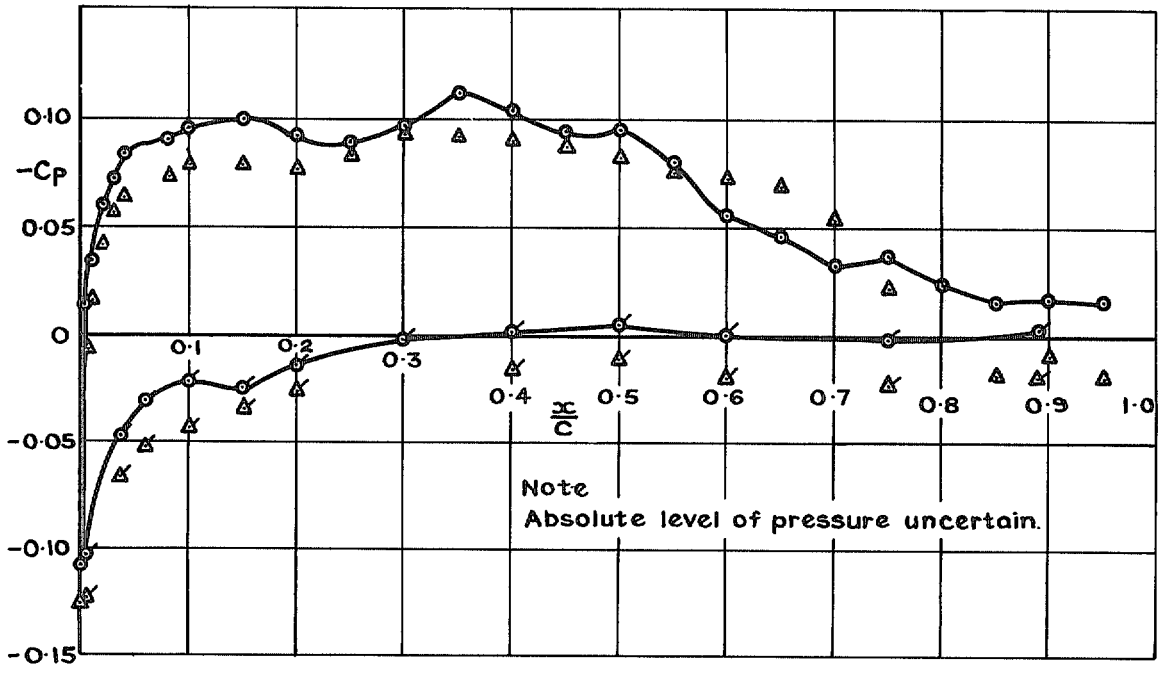

(b) With tufts $\alpha = 2{\cdot}0$ degrees

FIG. 3. Wing pressure distribution.

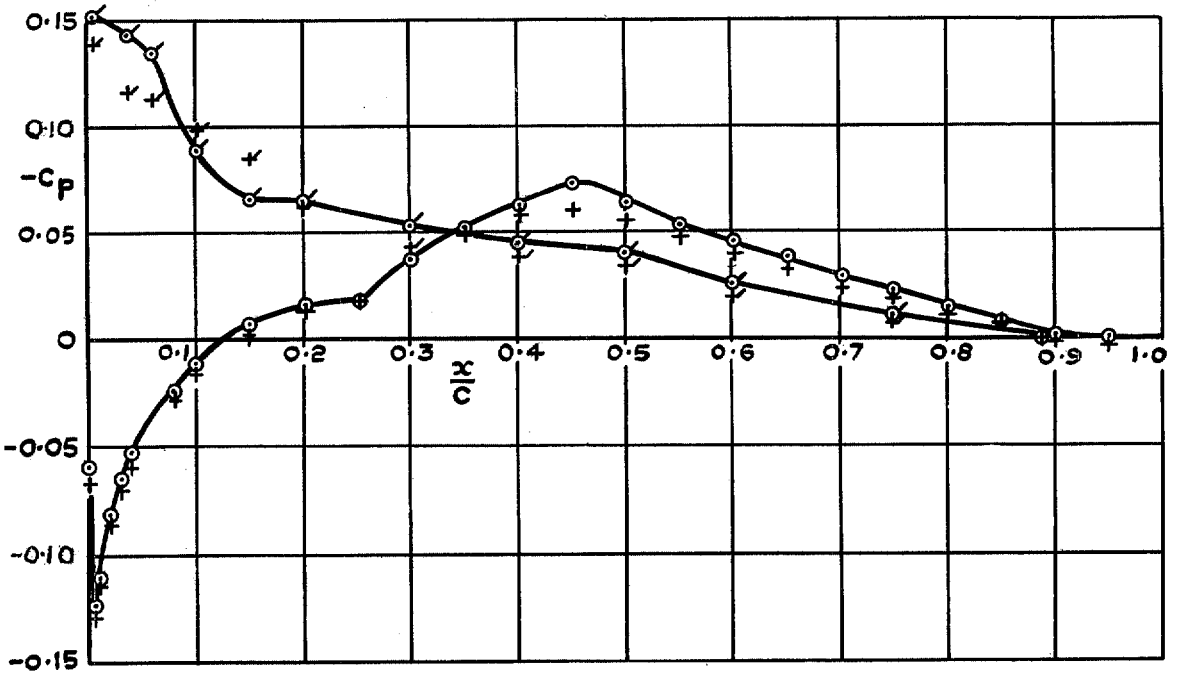

(c) $\alpha = -0.86$ degrees

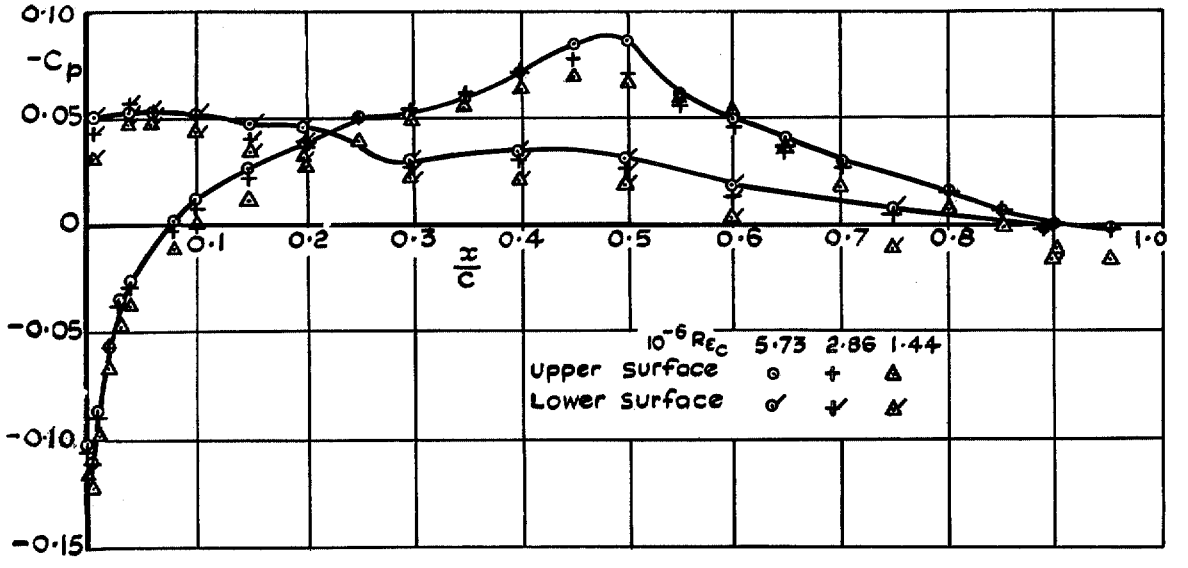

(d) $\alpha = 0$

FIG. 3 *contd.*

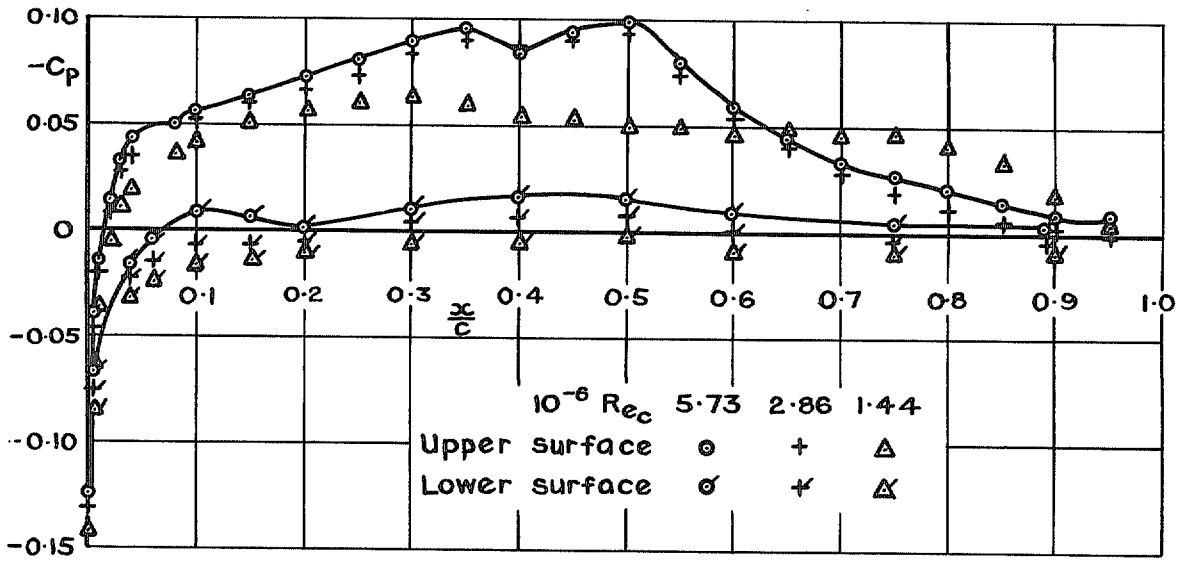

(e) $\alpha = 1{\cdot}3$ degrees

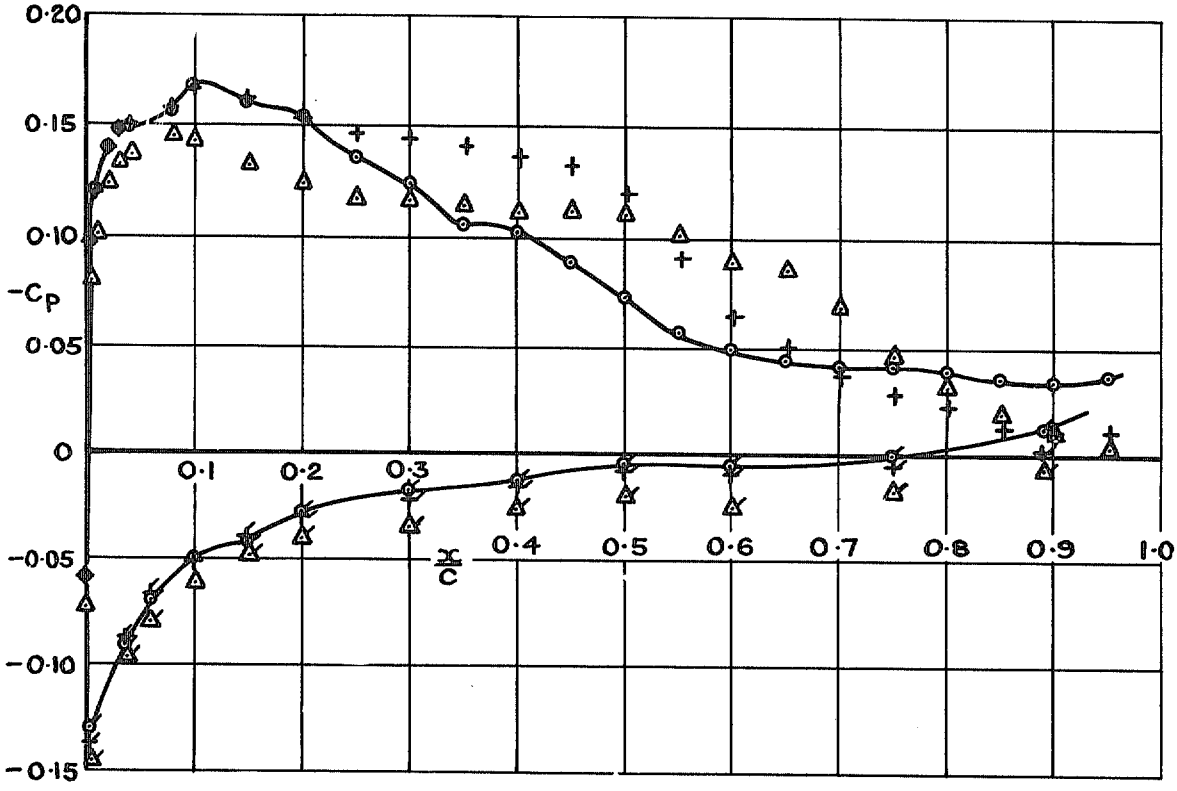

(f) $\alpha = 30$ degrees

FIG. 3 *concld.*

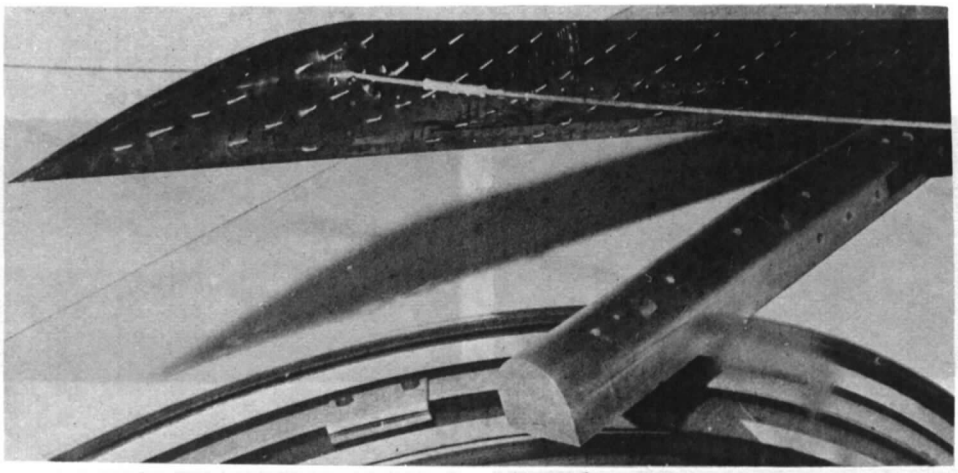

$Re_c = 5{\cdot}73 \times 10^6$

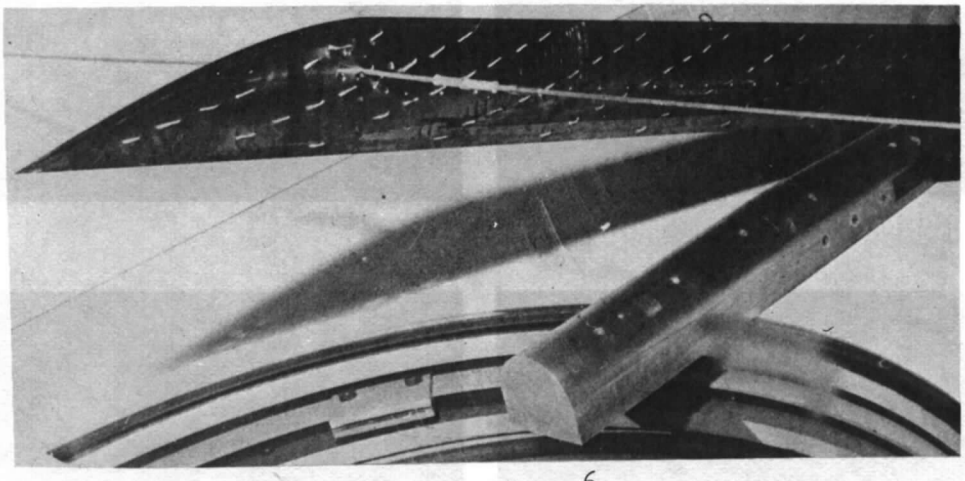

$Re_c = 2{\cdot}86 \times 10^6$

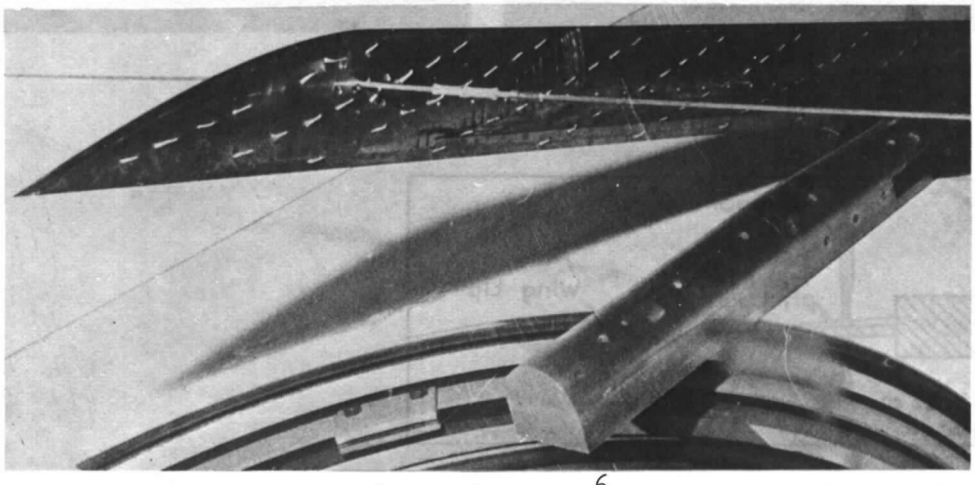

$Re_c = 1{\cdot}44 \times 10^6$

FIG. 4. Tufts on upper surface, $\alpha = 2$ degrees.

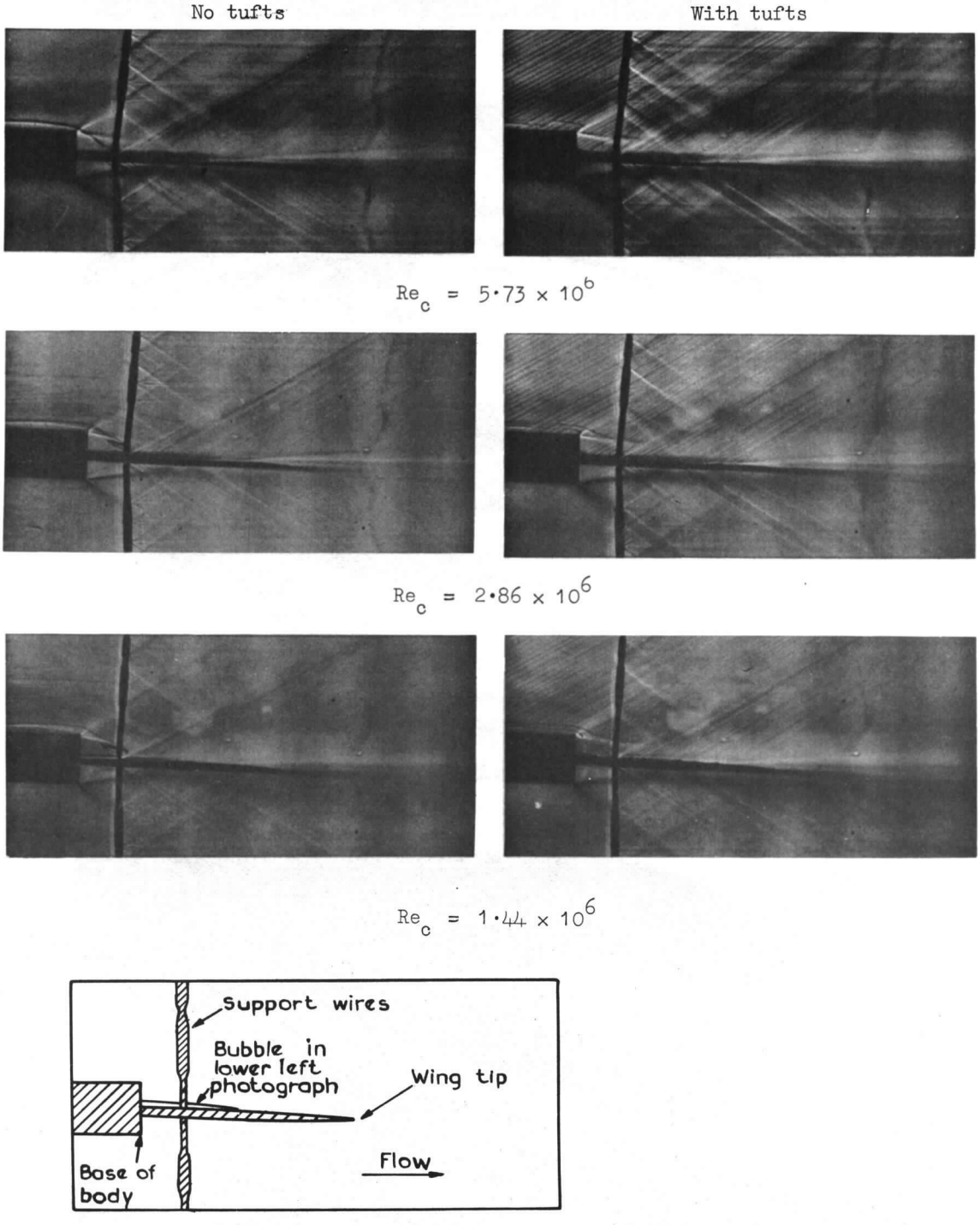

FIG. 5. Schlieren photographs, $\alpha = 2$ degrees.

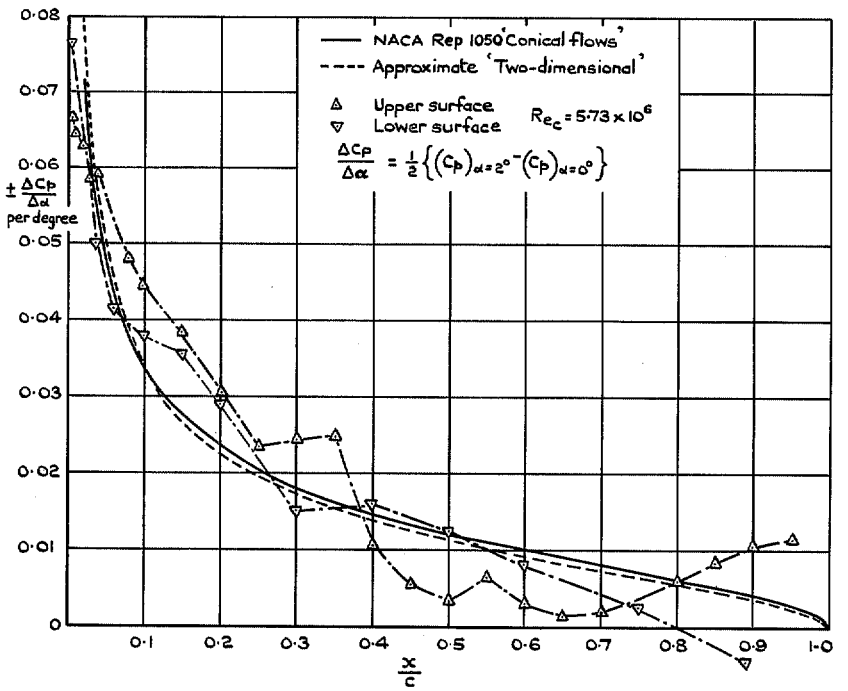

FIG. 6. Wing incidence loading.

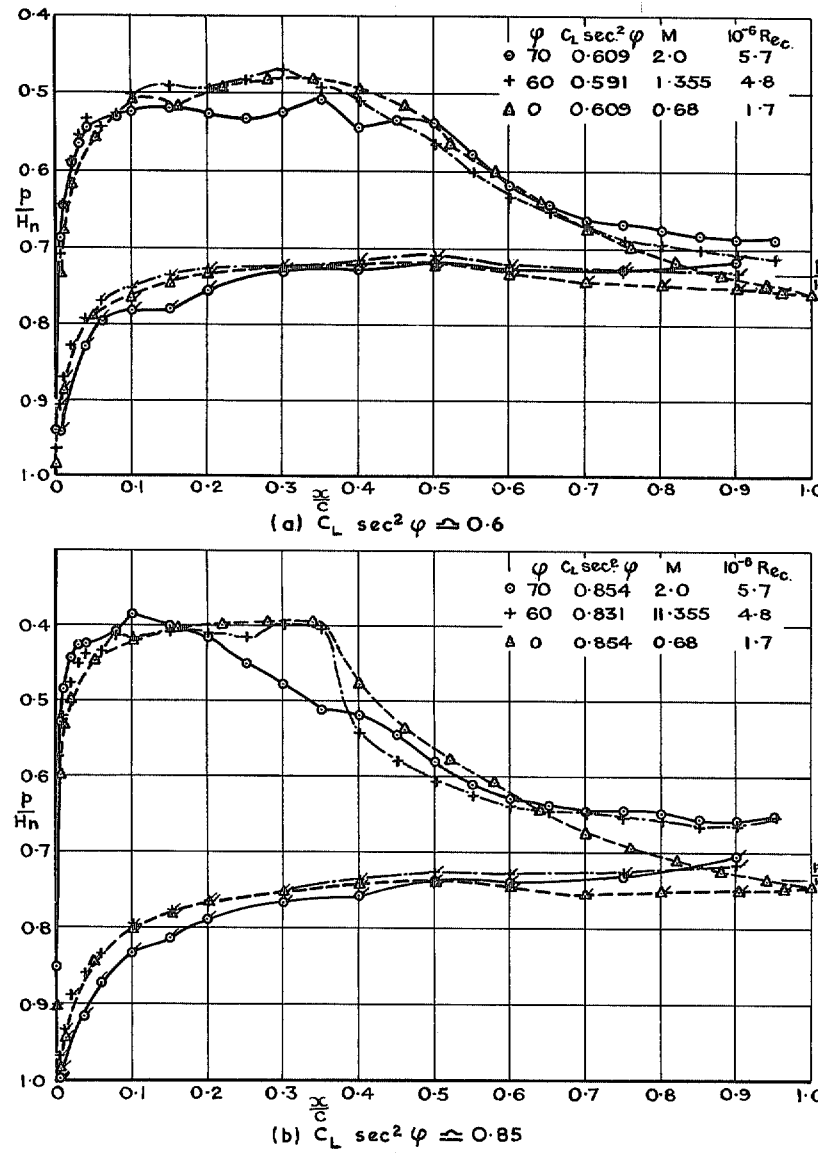

FIG. 7. Effect of sweepback on wing, pressure distribution.

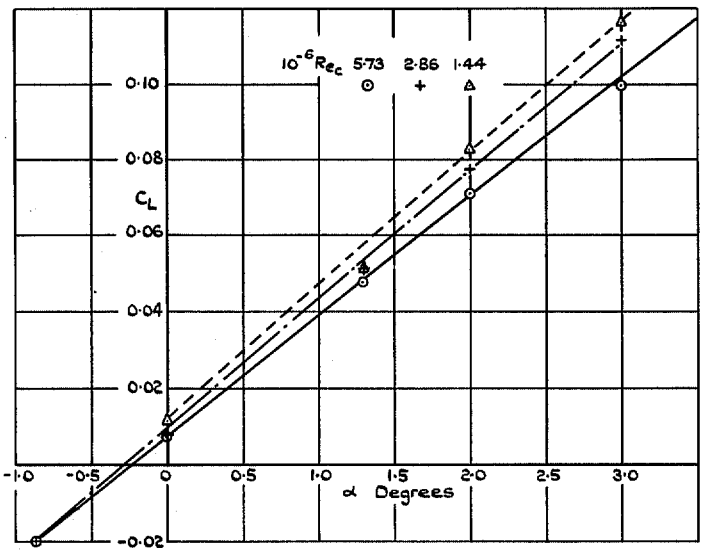

FIG. 8. Lift *vs* incidence.

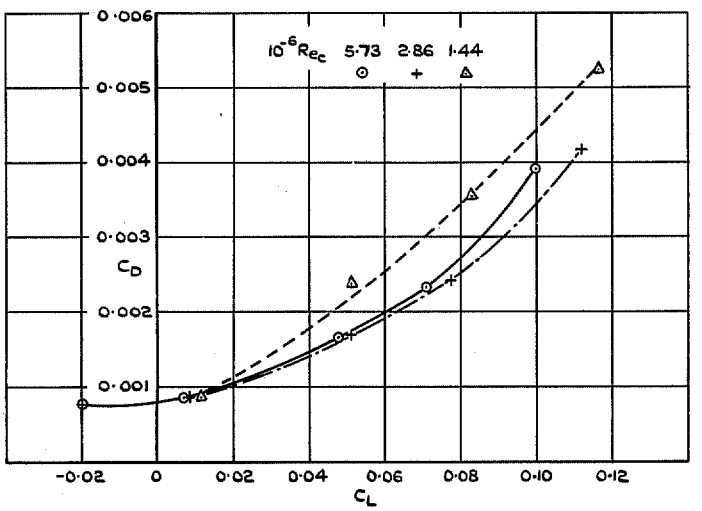

FIG. 9. Pressure drag *vs* lift.

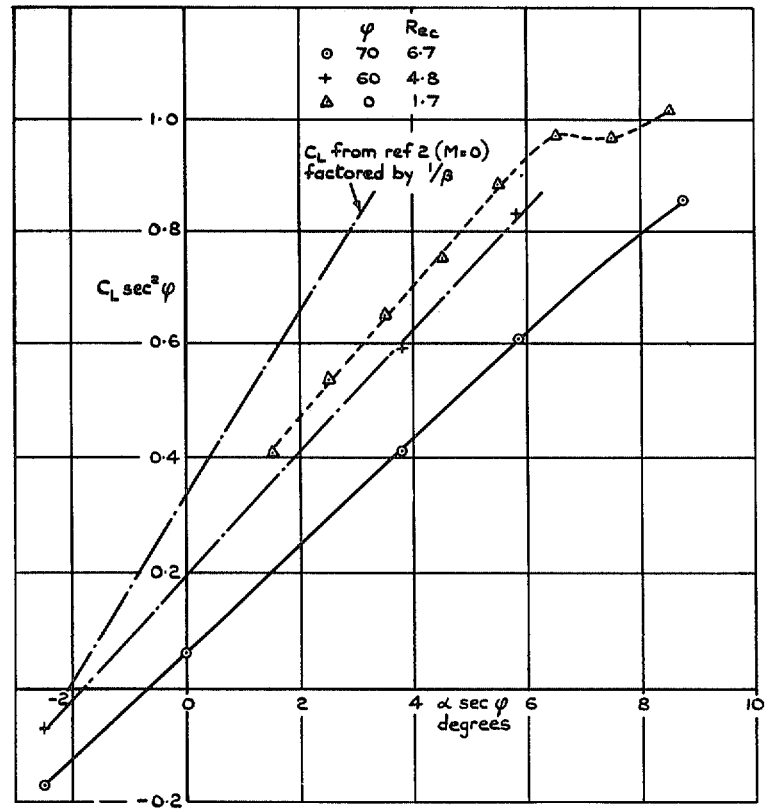

FIG. 10. Effect of sweepback on lift.

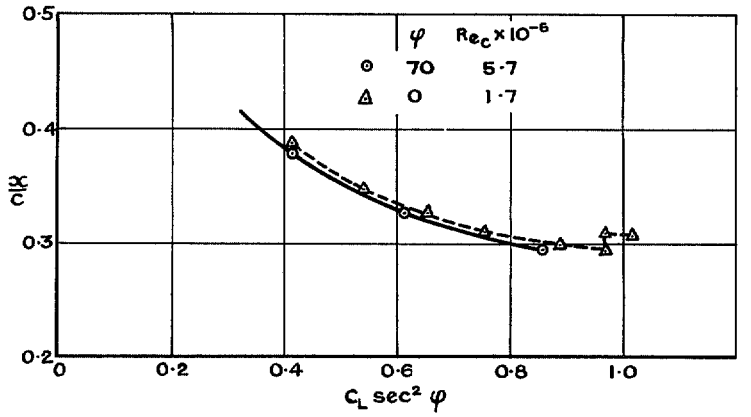

FIG. 11. Effect of sweepback on centre of pressure position.

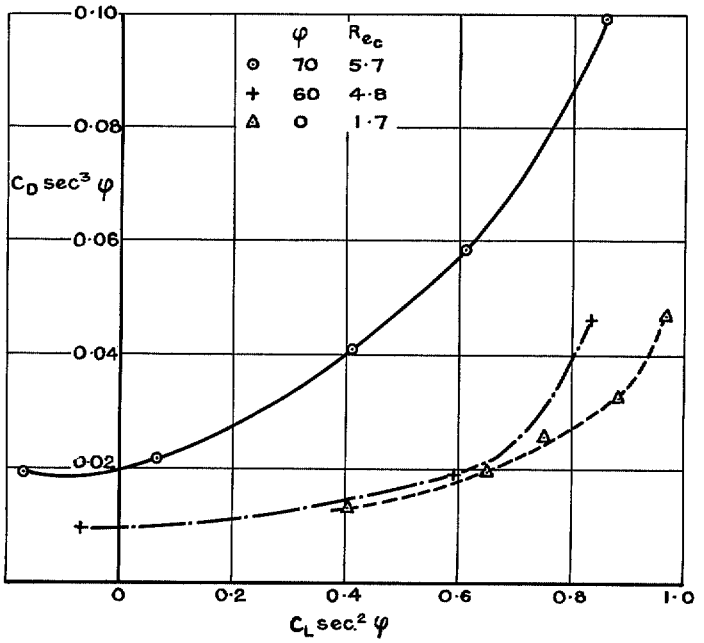

FIG. 12. Effect of sweepback on pressure drag.

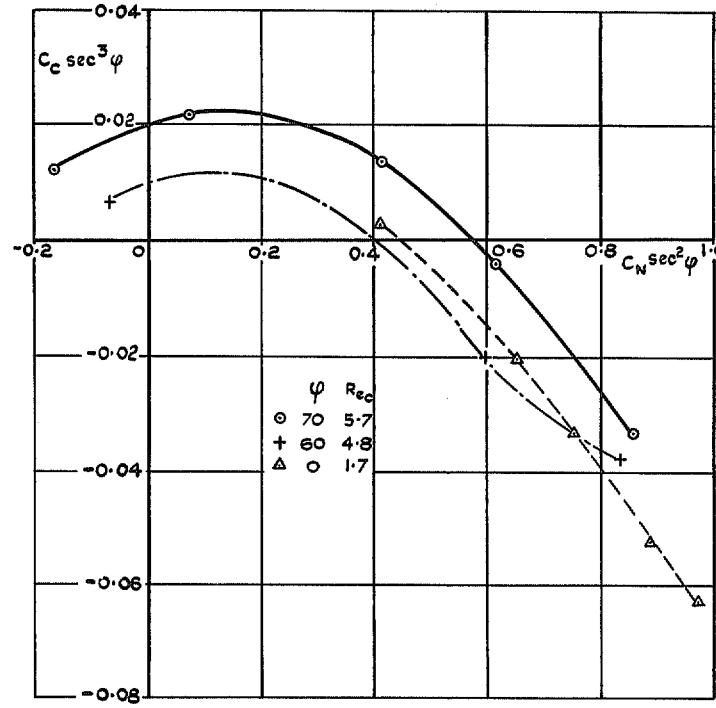

FIG. 13. Normal and chordwise components of pressure forces.

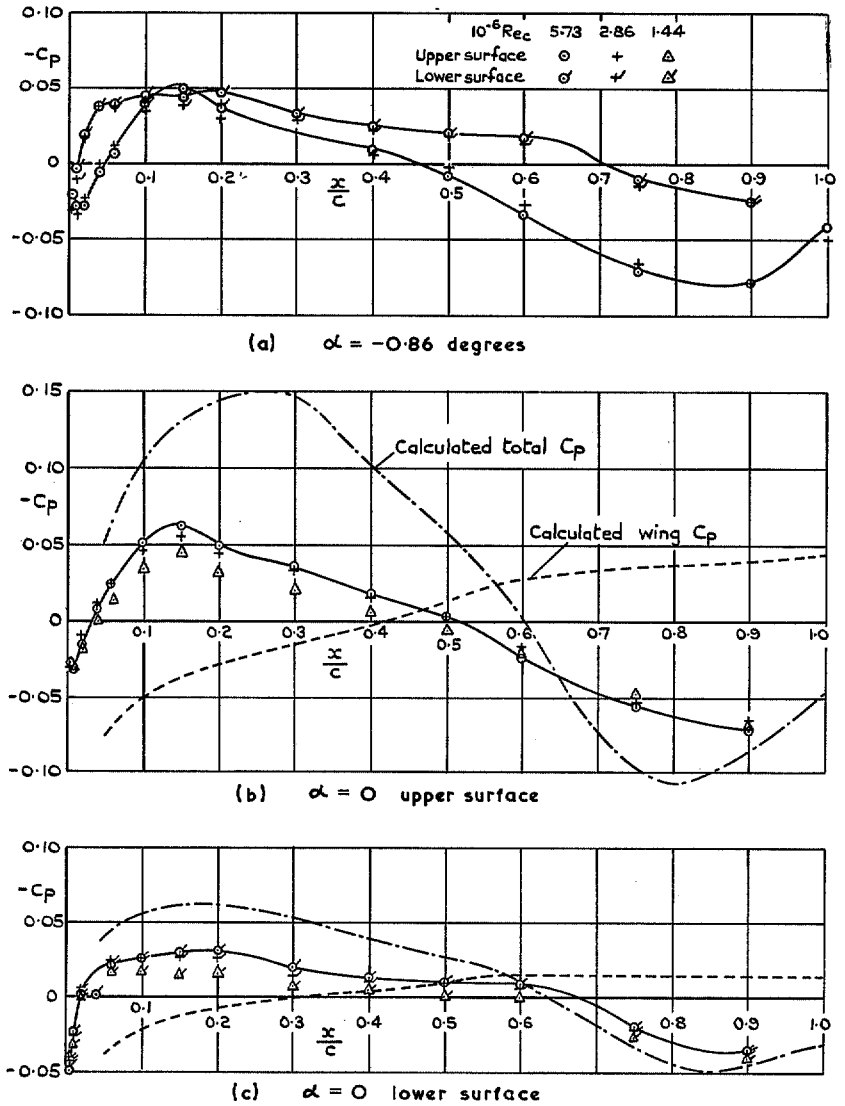

FIG. 14. Pressure distribution in wing-body junction.

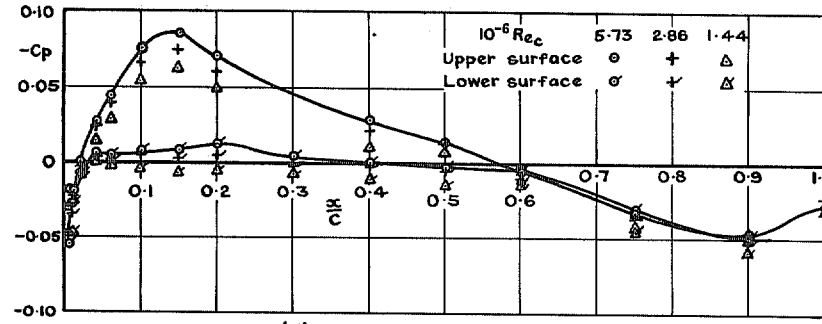

(d) $\alpha = 1{\cdot}3$ degrees

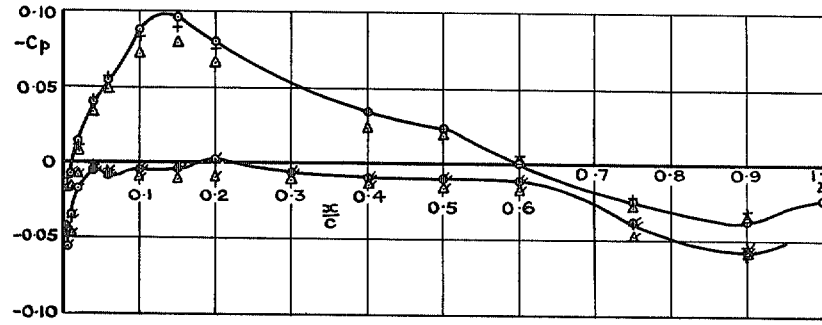

(e) $\alpha = 2{\cdot}0$ degrees

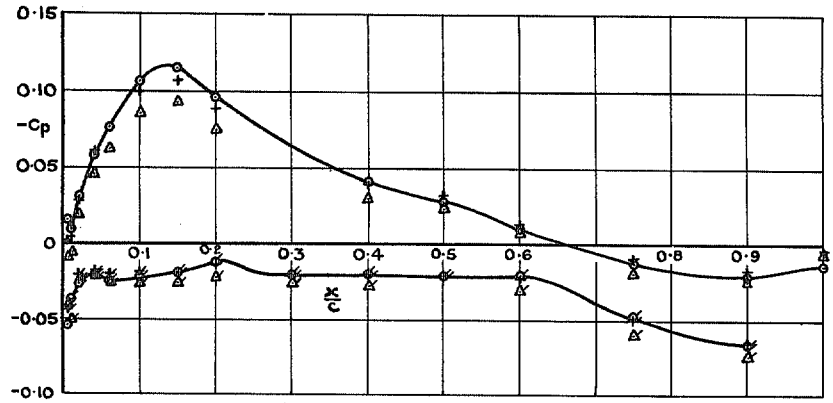

(f) $\alpha = 3{\cdot}0$ degrees

FIG. 14 *contd.*

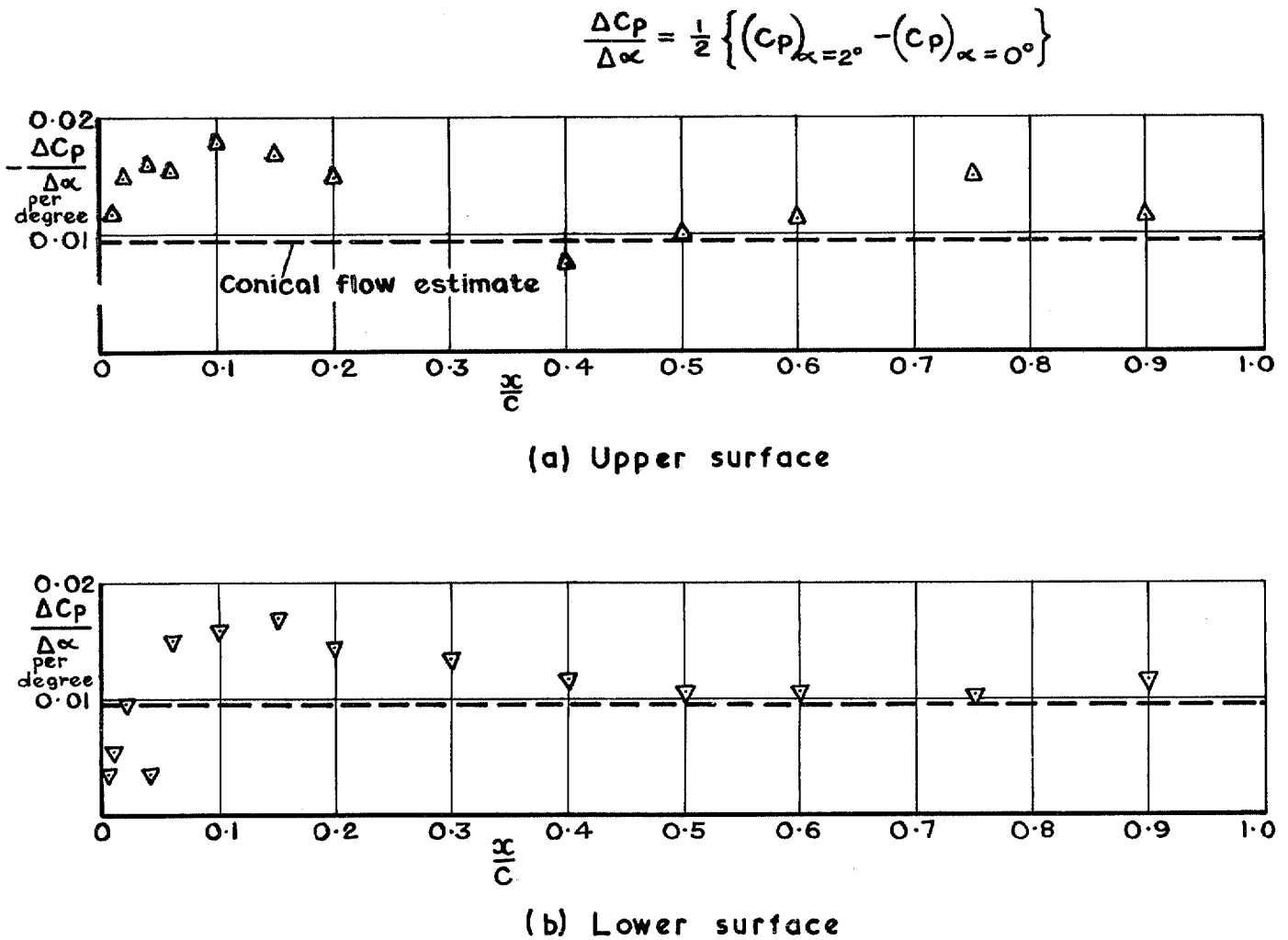

FIG. 15. Incidence loading in wing-body junction.

Printed in Wales for Her Majesty's Stationery Office by Allens Printers (Wales) Limited

Dd. 501372 K.5

Published by
HER MAJESTY'S STATIONERY OFFICE

To be purchased from
49 High Holborn, London WC1V 6HB
13a Castle Street, Edinburgh EH2 3AR
109 St Mary Street, Cardiff CF1 1JW
Brazennose Street, Manchester M60 8AS
50 Fairfax Street, Bristol BS1 3DE
258 Broad Street, Birmingham B1 2HE
80 Chichester Street, Belfast BT1 4JY
or through booksellers

R. & M. No. 3661
SBN 11 470401 5